SEC

AD-A264 289

(2)

ORT DOCUMENTATION PAGE

DTIC ELECTE MAY 13 1993 S C D

1a. REPORT SECURITY CLASSIFICATION UNCL	1b. RESTRICTIVE MARKINGS
2a. SECURITY CLASSIFICATION AUTHORITY	3. DISTRIBUTION/AVAILABILITY OF REPORT Approved for public release; distribution is unlimited
2b. DECLASSIFICATION/DOWNGRADING SCHEDULE	
4. PERFORMING ORGANIZATION REPORT NUMBER(S) NMRI 93-17	5. MONITORING ORGANIZATION REPORT NUMBER(S)
6a. NAME OF PERFORMING ORGANIZATION Naval Medical Research Institute 6b. OFFICE SYMBOL (If applicable)	7a. NAME OF MONITORING ORGANIZATION Naval Medical Command
6c. ADDRESS (City, State, and ZIP Code) 8901 Wisconsin Avenue Bethesda, MD 20889-5055	7b. ADDRESS (City, State, and ZIP Code) Department of the Navy Washington, DC 20372-5120
8a. NAME OF FUNDING/SPONSORING ORGANIZATION Naval Medical Research & Development Command 8b. OFFICE SYMBOL (If applicable)	9. PROCUREMENT INSTRUMENT IDENTIFICATION NUMBER
8c. ADDRESS (City, State, and ZIP Code) 8901 Wisconsin Avenue Bethesda, MD 20889-5044	10. SOURCE OF FUNDING NUMBERS PROGRAM ELEMENT NO. 62233N; PROJECT NO. MM33C30.005; TASK NO. 1051; WORK UNIT ACCESSION NO. DN249507

11. TITLE (Include Security Classification)
Measurements of cell physiology: ionized calcium, pH, and glutathione

12. PERSONAL AUTHOR(S)
Rabinovitch PS, June CH, Kavanagh TJ

13a. TYPE OF REPORT	13b. TIME COVERED	14. DATE OF REPORT (Year, Month, Day)	15. PAGE COUNT
Book chapter	FROM _____ TO _____	1993	30

16. SUPPLEMENTARY NOTATION In: Clinical Flow Cytometry: Principles and Application. Edited by Kenneth D. Bauer, Ricardo E. Duque, T. Vincent Shankey. Baltimore: Williams & Wilkins. 1992 pp. 505-534

17. COSATI CODES			18. SUBJECT TERMS (Continue on reverse if necessary and identify by block number)
FIELD	GROUP	SUB-GROUP	flow cytometry; calcium; pH; HIV infection; signal transduction

19. ABSTRACT (Continue on reverse if necessary and identify by block number)

93 5 10 011

93-10214

20. DISTRIBUTION/AVAILABILITY OF ABSTRACT	21. ABSTRACT SECURITY CLASSIFICATION
☒ UNCLASSIFIED/UNLIMITED ☐ SAME AS RPT. ☐ DTIC USERS	Unclassified
22a. NAME OF RESPONSIBLE INDIVIDUAL Phyllis Blum, Librarian.	22b. TELEPHONE (Include Area Code) (301) 295-2188 22c. OFFICE SYMBOL MRL/NMRI

DD FORM 1473, 84 MAR 83 APR edition may be used until exhausted. All other editions are obsolete.

SECURITY CLASSIFICATION OF THIS PAGE
UNCLASSIFIED

31

Measurements of Cell Physiology: Ionized Calcium, pH, and Glutathione

PETER S. RABINOVITCH, CARL H. JUNE, and TERRANCE J. KAVANAGH

The flow cytometer can be used to measure a variety of functional parameters that are of increasing interest to cell biologists. The recent development of a number of new fluorescent probes now permits the measurement of various intracellular free ion concentrations in single living cells. Among these ions are calcium, magnesium, sodium, potassium, and hydrogen (pH). In addition, intracellular glutathione, crucial for maintaining the physiological redox state, can be easily and accurately measured by flow cytometry. Most previously available techniques to measure cellular activation parameters determined the mean value for a mixed population of cells. The flow cytometer has the unique capacity to permit the measurement of physiologic parameters in large numbers of single cells; it allows correlation with other parameters, such as immunophenotype and cell cycle; and, finally, it reveals heterogeneity within the cell population, sometimes even in cells that were previously thought to be homogeneous. In this chapter, flow cytometric techniques to measure intracellular calcium concentration, pH, and glutathione as well as their applications are described.

INTRACELLULAR IONIZED CALCIUM

Introduction

Eukaryotic cells in their resting state maintain an internal calcium ion concentration that is far below that of the extracellular environment. Ionized calcium has an important role as a mediator of transmembrane signal transduction, and elevations in intracellular ionized calcium concentration ($[Ca^{2+}]_i$) regulate diverse cellular processes. Measurement of $[Ca^{2+}]_i$ in living cells is thus of considerable interest to investigators over a broad area of immunology and cell biology.

Calcium influx is thought to be initiated by membrane depolarization, which opens voltage-gated channels, or by the binding of ligands to receptor-operated channels. The latter case is more commonly encountered by investigators using flow cytometry, as these mechanisms predominate in cells that are not electrically excitable; in this case, the binding of agonist to its specific membrane receptor activates enzymatic processes that result in the activation of phospholipase C. In many cases, this process requires the intervening activation of a guanine nucleotide binding (G) protein. Phospholipase C causes the hydrolysis of a membrane phospholipid, phosphatidylinositol 4,5-bisphosphate (PIP2), which yields a water soluble product, inositol 1,4,5-trisphosphate (IP3), and a lipid, 1,2-diacylglycerol (DAG). IP3 then causes the release of calcium from intracellular stores while DAG, in conjunction with calcium ions, activates protein kinase C. Thus, a single agonist can result in the production of at least two "second messengers," making this pathway a unique, bifurcating system. Calcium is therefore a "third messenger" that controls numerous cellular processes, activating a broad variety of enzyme systems, both as a cofactor and in conjunction with the calcium-binding protein calmodulin. While it appears clear that the initial elevation of ionized calcium is due to the release of intracellular calcium stores, little is known about regulation of the influx of calcium from extracellular sources that is necessary to sustain the response.

Indicators of Intracellular Ionized Calcium Concentration

Until 1982, it was not possible to measure $[Ca^{2+}]_i$ in small intact cells and attempts to measure cytosolic free calcium were restricted mostly to large invertebrate cells where the use of microelectrodes was possible. Bioluminescent indicators, such as aequorin, a calcium–sensitive photoprotein, are well suited for certain applications (1). Their greatest limitation is the necessity for loading into cells by microinjection or other forms of plasma membrane disruption. $[Ca^{2+}]_i$ was first measured in diverse populations of cells with the development of quin2 (2). The indicator was easily loaded into small intact cells using a chemical technique developed by Tsien (3). Cells are incubated in the presence of the acetoxymethyl ester of quin2. This uncharged form is cell permeant and diffuses freely into the cytoplasm, where it serves as a substrate for esterases. Hydrolysis releases the tetraanionic form of the dye that is trapped inside the cell. Unfortunately, quin2 has several disadvantages that limit its application to flow cytometry (4). Its relatively low extinction coefficient and quantum yield have made detection of the dye at low concentrations difficult; at higher concentrations, quin2 itself

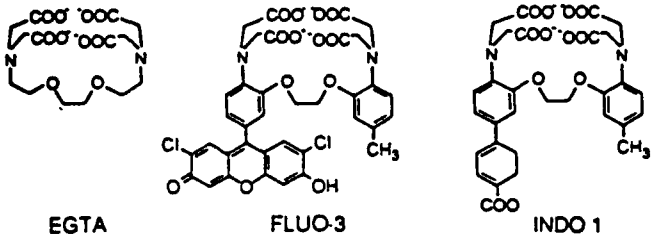

Figure 31.1. Structure of the $[Ca^{2+}]_i$ probes *indo-1* and *fluo-3* as well as, for reference, the structure of the calcium chelator *EGTA*. Note the identical calcium-binding domain in all three compounds.

buffers the $[Ca^{2+}]_i$. Subsequently, Grynkiewicz et al. (5) described a new family of highly fluorescent calcium chelators that overcome most of the above limitations. One of these days, indo-1 ([1-[2amino-5-[6-carboxylindol-2-yl]-phenoxy]-2-[2'-amino-5'-methlyphenoxy] ethane N,N,N'N'-tetraacetic acid]) (Fig. 31.1), has spectral properties that make it especially useful for analysis with flow cytometry. In particular, indo-1 exhibits large changes in fluorescent emission wavelength upon calcium binding (Fig. 31.2). As described below, use of the ratio of intensities of fluorescence at two wavelengths allows calculation of $[Ca^{2+}]_i$ independent of variability in cellular size or intracellular dye concentration. The only significant drawback to the use of indo-1 is the requirement for ultraviolet (UV) excitation.

A practical alternative to *indo-1 became available upon* the description by Minta et al. (6) of a fluorescein-based, calcium-sensitive probe, fluo-3 (Fig. 31.1). This dye exhibits an increase in fluorescence intensity with increasing $[Ca^{2+}]_i$ (Fig. 31.3). Fluo-3 is less sensitive than quin2 and indo-1 at detecting small changes in $[Ca^{2+}]_i$, in part, because the Kd is higher (400 nM); conversely, this may be an advantage if the experimental situation involves the distinciton between stimuli, all of which produce large (above 400 nm) $[Ca^{2+}]_i$ responses. An additional advantage with fluo-3 is that it can be used with other probes such as caged calcium chelators that may themselves require UV excitation (7). Furthermore, the use of fluo-3 permits, for the first time, the simultaneous use of other UV-excitable probes for flow cytometry, such as those used for cell cycle analysis or measurement of intracellular glutathione, allowing correlation of these parameters with calcium responses. The primary disadvantage of fluo-3 is that it does not have fluorescence properties that allow ratiometric determinations. Therefore, calibration on a flow cytometer is more complicated because the signal is proportional to cell size and dye concentration as well as $[Ca^{2+}]_i$. Thus, the ability to measure responses in subsets of cells is more limited because the broad distribution of fluorescence intensities of unstimulated cells often results in an overlapping distribution of the values from stimulated and unstimulated cells. This problem can be minimized by loading cells in the presence of pluronic F-127 (see below), which minimizes the cell-to-cell variation in loading with fluo-3 (8), or by the simultaneous use of a second dye that serves as an indicator of the magnitude of dye loading in an individual cell. Rijkers et al. (9) have suggested using the ratio of fluo-3 to SNARF-1 (SemiNaphthoRhodaFluor) fluorescence for this purpose (see subsequent section on pH).

Preparation of Cells for Indo-1 or Fluo-3 Analysis

Uptake and retention of indo-1 and fluo-3 is facilitated by the use of their penta-acetoxymethyl esters, using the scheme described above. Approximately 20% of the total dye is trapped in this manner during typical loadings. After loading, the extracellular dye should be diluted 10- to 100-fold before flow cytometric analysis (10). A typical protocol for cell preparation might be:

1. Incubate $0.5 - 20.0 \times 10^6$ cells/ml in medium with $1 - 3$ μM fluo-3 or indo-1 (acetoxymethyl esters) at 37°C for 30 min. For cells that are difficult to load, or that result in heterogeneous loading, 0.02% (final vol/vol) pluronic detergent F-127 (Molecular Probes) may be added to the above before incubation, with subsequent incubation at 30°C (11, 12). An additional option for the use of fluo-3 is to retard transport of the deesterified dye out of the cell by adding 4 mM (final concentration) probenecid during loading. In initial experiments, we suggest using lymphocytes, as they are easily and reliably loaded. Later, when the technique is validated on the flow cytometer, other cell types can be utilized.
2. For experiments with simultaneous immunofluorescence, incubate aliquots of the above with saturating concentrations of R-phycoerythrin (PE)-conjugated antibody (with fluo-3) or fluorescein isocyanate (FITC)- and/or PE-conjugated antibody (with indo-1) at room temperature for 30 min. Antibodies should be azide-free in order not to poison cellular metabolism.
3. Centrifuge the above for 6 min at 180g at room temperature. Gently resuspend (do not vortex) in medium at the desired cell concentration (usually $\sim 10^6$/ml) at room temperature. The medium used for resuspension and analysis can be dictated primarily by the metabolic requirements of the cells, subject only to reasonable pH buffering (preferably not solely bicarbonate, as it will become alkaline) and the requirement that mM concentrations of calcium be present. If analysis of Ca^{2+} released from intracellular stores (independent of influx of extracellular Ca^{2+}) is desired, addition of 5 mM EGTA (ethylene glycol bis (β-aminoethyl ether)-N,N,N',N'-tetraacetic acid) to the cell suspension will reduce Ca^{2+} to ~20 nM, thus abolishing the usual cross-membrane gradient.
4. Hold cells at room temperature (~22°C) until ready for analysis. Leakage and compartmentalization of both dyes is accelerated at higher temperatures. Warm an aliquot of cells to 37°C for at least 5 min before analysis. Analyze at 37°C. For a 10-min analysis, use at least 0.5 ml (usually containing $\sim 10^6$ cells), so that cell transit is rapid from the warm sample chamber to the flow cell (this is usually through unheated small caliber tubing). $[Ca^{2+}]_i$ responses are highly temperature-dependent and reduced or even absent calcium responses will be seen at lower temperatures.
5. After obtaining a baseline measurement for a sample, kinetic analyses are typically performed by quickly ceasing flow, removing the sample container, adding agonist, and rapidly restarting flow (more sophisticated and rapid sample injection schemes are possible, but for the great majority of applications, the above will suffice).

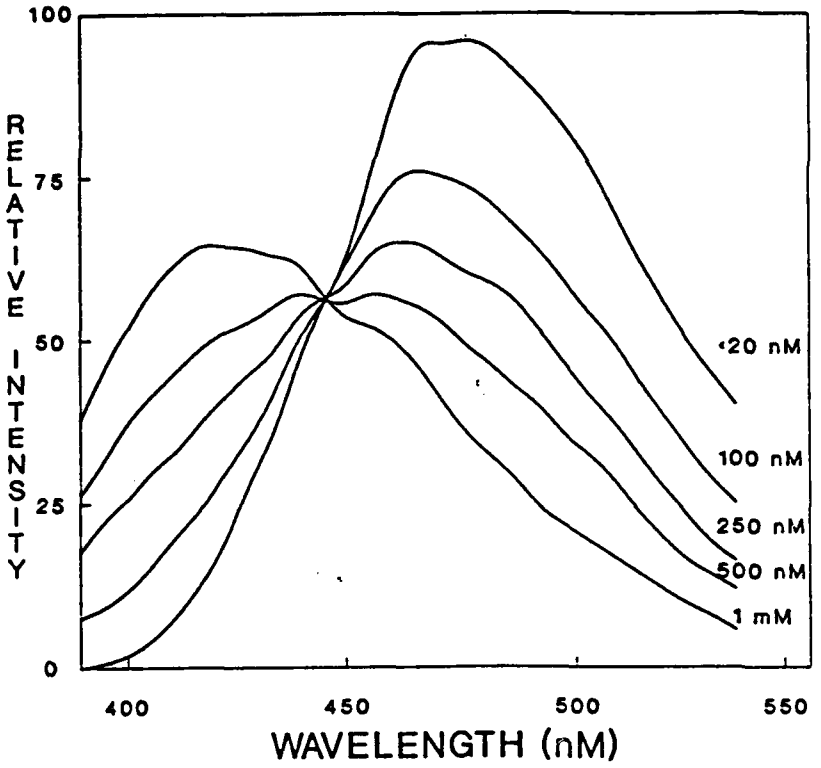

Figure 31.2. Emission spectra for indo-1 as a function of ionized calcium concentration. Fluorescence excited at 356 nm was measured in a spectrofluorimeter. At wavelengths below 400 nm, emission in the absence of calcium drops to a few percent of that seen in the pres ence of calcium. About 500 nm, there is more than a fourfold converse difference. The $[Ca^{2+}]$ of EGTA buffer solutions used is shown at the right.

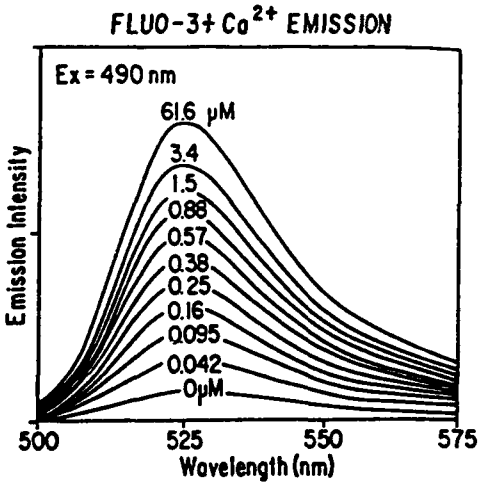

Figure 31.3. Emission spectra for fluo-3 as a function of ionized calcium concentration. The concentration of Ca^{2+} in the buffer solutions is indicated for each individual spectrum. (Courtesy of R. Haugland, Molecular Probes, Eugene, OR).

6. Calibrate using one of the approaches discussed subsequently. If using ionomycin, it is necessary to be scrupulous in removing residual ionophore before analyzing the next sample. Use washes with bleach and/or dimethyl sulfoxide (DMSO) to facilitate the removal of traces of ionomycin.

One incidental benefit of the above loading strategy is that this procedure, like the more familiar use of fluorescein diacetate or carboxyfluorescein diacetate, allows one to distinguish between live and dead cells. The latter will not retain the hydrophilic impermeant dye and can be excluded by gating during subsequent analysis. The lower limit of useful intracellular loading concentrations of both indo-1 and fluo-3 is determined by the sensitivity of fluorescence detection of the flow cytometer, and the upper limit is determined by avoidance of buffering of $[Ca^{2+}]_i$ by the presence of the calcium chelating dye itself. In practice, one should use the least amoung of dye that is necessary to reliably quantitate the fluorescence signal. In the case of indo-1, the dye has excellent fluorescence characteristics (30-fold greater quantum yield than quin2; (5) and useful ranges of indo-1 loading are much lower than the millimolar amounts required with quin2. In using the newer dye fluo-3, one should begin with the same lower concentration that is found to be suitable with indo-1 and increase loading only if detection against background autofluorescence becomes limiting (autofluorescence in the green spectrum is greater than in the blue or violet spectrum used by indo-1). For human peripheral blood T-cells, we have found adequate detection of both dyes at or above 1 μM (for indo-1 intracellular concentrations achieved with this loading are ~5 μM). Buffering of $[Ca^{2+}]_i$ in human T-cells can be observed as a slight delay in the rise in $[Ca^{2+}]_i$ and a retarded rate of return of $[Ca^{2+}]_i$ to baseline values. In the case of indo-1, this was seen when loading concentrations above 3 μM (22 μM intracellular concentration) were used. A reduction in peak $[Ca^{2+}]_i$ occurred at even higher indol-1 concentrations (10). Chused et al. (13) have observed slightly greater sensitivity of murine B-cells to indo-1 buffering, recommending a loading concentration of no

greater than 1 μM. In side by side comparisons, we have found that calcium transients in B-cells are much more sensitive to the effects of buffering by indo-1 than are T-cells. For human platelets, a 2 μM indo-1 loading concentration has been reported (14). Rates of loading of the dye esters can be expected to vary between cell types, perhaps as a consequence of variations in intracellular esterase activity. In peripheral human blood, more rapid rates of loading are seen in platelets and monocytes than in lymphocytes. Even within one cell type, donor- or treatment-specific factors may affect loading; for example, lower rates of indo-1 loading are seen in splenocytes from aged mice than from young mice (15).

Indo-1 has been found to be remarkably nontoxic to cells subsequent to loading. Analysis of the proliferative capacity of human T-lymphocytes (10) loaded with indo-1 has shown no adverse effects on the ability of cells to enter and complete three rounds of the cell cycle. Similar results have been obtained with murine B-lymphocytes (13). This is especially pertinent to the viable sorting of indo-1 loaded cells based on $[Ca^{2+}]_i$, as described subsequently.

Flow Cytometric Analysis Technique

The instrumental setup for fluo-3 analysis is simply that used for routine FITC analysis, i.e., 488 nm excitation and detection of emission in a band centered near 525 nm. Considerations for indo-1 analysis are slightly more complex. The absorption maximum of indo-1 is between 330 and 350 nm, depending upon the presence of calcium (5); this is well suited to excitation at either 351–356 nm from an argon-ion laser, or 337–356 nm from a krypton-ion laser, and (although spectrally slightly less optimal) almost the same performance can be obtained by excitation at 325 nm using a helium-cadmium Laser. Laser power requirements depend upon the choice of emission filters and the optical efficiency of the instrument; however, under optimal optical conditions (i.e., using quartz flow cells) as little as 5–10 mW excitation appears satisfactory, within the range available from helium-cadmium lasers. In this regard, the stability of the intensity of the excitation source is less important in this application because of the use of the ratio of fluorescence emissions.

An increase in $[Ca^{2+}]_i$ is detected with indo-1 as an increase in the ratio of fluorescence intensity from a lower to a higher emission wavelength. The optimal strategy is to select bandpass filters so that the collection of light near the isosbestic point is minimized and the collection of fluorescence that exhibits the largest variation in calcium–sensitive emission is maximized. The choice of filters used to select these wavelengths is dictated by the spectral characteristics of the shift in indo-1 emission upon binding to calcium (Fig. 31.2). The original spectral curves published for indo-1 (5) did not depict the large amounts of indo-1 emission in the blue-green and green wavelengths; in practice, we find that there is more light available in the blue region than in the violet region, although the dynamic range of the calcium-sensitive changes in the violet region exceeds that of the blue region (Fig. 31.2). The choice of filter combinations can lead to substantial differences in the magnitude of observed changes in the violet-blue ratio, perhaps best summarized by the value R_{max}/R, the range of change in indo-1 ratio observed from resting intracellular calcium (R) to saturated calcium (R_{max}). Filters centered at 530 nm (green) and 395 nm (violet) result in a R_{max}/R ratio of 9.0 (individual instruments may vary somewhat). Replacing the 395-nm emission filter with one centered on the peak "violet" emission of the calcium-bound indo-1 dye (405 nm) reduces R_{max}/R to 7.9. Instead, replacing the 530-nm filter with one centered on the peak "blue" emission of calcium-free indo-1 dye (485 nm) reduces R_{max}/R to 6.6. Thus, a greater dynamic range of the indo-1 ratio is observed when light nearer to the isosbestic (450 nm) is avoided. Note that if a 525- to 530-nm bandpass filter is used for the longer indo-1 emission wavelength, then this same filter and photomultiplier tube can be used for (temporally displaced and gated) FITC emission.

Calibration of Fluorescence to $[Ca^{2+}]_i$

Prior to the development of indo-1, $[Ca^{2+}]_i$ determination with quin2 fluorescence was sensitive to cell size and intracellular dye concentration as well as $[Ca^{2+}]_i$. This made necessary the calibration of each loaded sample (in fact, strictly speaking of each individual assay) by determination of the fluorescence intensity of the dye at known Ca^{2+} concentrations, or at least at zero and saturating Ca^{2+}. This is still the case for analyses with fluo-3. In contrast, with indo-1, use of the Ca^{2+}-dependent shift in dye emission wavelength allows the ratio of fluorescence intensities of the dye at the two wavelengths to be used to calculate $[Ca^{2+}]_i$:

$$[Ca^{2+}]_i = Kd \cdot \frac{(R - R_{min})}{(R_{max} - R)} \cdot \frac{S_{f2}}{S_{b2}} \qquad \text{[Eq. 31.1]}$$

where Kd is the effective dissociation constant (250 nM at 37°C, pH 7.05), R, R_{min}, and R_{max} are the fluorescence intensity ratios of violet-blue fluorescence at the experimental, zero, and saturating $[Ca^{2+}]_i$, respectively; and S_{f2}/S_{b2} is the ratio of the blue fluorescence intensity of the calcium-free and calcium-bound dye, respectively (5). Note that the Kd varies dramatically as a function of temperature, pH, and ionic strength. The term S_{f2}/S_{b2} is a constant that depends in largest part on the filters used for indo-1 analysis. Determination of R_{max}, R_{min} and S_{f2}/S_{b2} for calibration of indo ratios allows the direct determination of $[Ca^{2+}]_i$ using the above equation. Determintion of R_{max} is easily performed by addition of the calcium ionophore ionomycin to a cell sample (1–3 μg/ml final). Unfortunately, simply adding EGTA to cells treated with ionomycin and metabolic poisons does not reduce the fluorescence ratio of cells to R_{min}. The details of a strategy that makes use of a spectrofluorimeter in addition to the flow cytometer has been previously described (10). Because the ratiometric analysis is independent of cell size and total intracellular dye concentration as well as of instrumental variation in efficiency of excitation or emission detection,

it is not necessary to measure the fluorescence of the dye in the calcium-free and calcium-saturated states for each individual assay. In principle, it is sufficient to calibrate the instrument once, after which only R is measured for each subsequent analysis. In practice, the minimum quality control should include determination of the value of R_{max}/R (cells treated with ionomycin/resting cells) for each experiment; day-to-day optical variations in the flow cytometer are usually minimal (with the same filter set) and, thus, a narrow range of R_{max}/R values should be obtained.

As an alternative to the combined use of a flow cytometer with a spectrofluorimeter, Parks et al. (16) have proposed that, with minor modification, the flow cytometer may be used as a spectrofluorimeter. In essence, the fluorescence of a steady stream of dye is measured by the photomultiplier and the photomultiplier voltage is analyzed as in a standard spectrofluorimeter, or, even beter, the voltage is electronically converted to a pulse for processing by the flow cytometer. An alternative approach to create such a pulse is to rapidly strobe the laser, such that the beam is illuminated for only μsec intervals. Preliminary experience with this technique suggests that it is possible to determine all of the constants necessary for calibration directly on the flow cytometer using EGTA-depleted and calcium-saturated indo-1 solutions.

An alternative approach to calibration can be based upon a regression curve that relates R to treated cells suspended in a series of precisely prepared calcium buffers. Chused et al. (13) have suggested that ionomycin plus a cocktail of metabolic poisons be used to collapse the calcium gradient to zero ($[Ca^{2+}]_i = [Ca^{2+}]_o$). Thus, this technique allows one to estimate $[Ca^{2+}]_i$ without the need to determine R_{min}, S_{f2} or S_{b2}, although it is subject to limitations in the precision with which one can prepare a series of calcium buffers that yield known and reproducible free calcium concentrations. Accuracy of prediction of ionized Ca^{2+} concentration in buffer solutions depends on a variety of interacting factors, so that care must be exercised in formulating Ca^{2+} standards. The ionized calcium concentration in an EGTA buffer system depends on the magnesium concentration; other metals such as aluminum, iron, and lanthanum also bind avidly to EGTA (17). In addition, the dissociation constant of Ca^{2+}-EGTA is a function of pH, temperature, and ionic strength (review 1, 19). For example, in an EGTA buffer (total EGTA 2 mM, total Ca^{2+} 1 mM, ionic strength 0.1 at 37°C), changing the pH from 7.4 to 7.0 can result in the ionized calcium increasing by more than 200 nM, a change that is approximately twice the magnitude of that found in resting cells and that is easily measured on a flow cytometer. Finally, it is important to prepare the buffers using the "pH metric technique" (19), in part because of the varying purity of commercially available EGTA (20). Detailed methods and a computer program that will determine $[Ca^{2+}]$ as a function of pH, total calcium and magnesium concentrations, temperature, and ionic strength are available from one of this chapter's authors (C. June). A practical alternative for obtaining buffers is made possible by the recent commercial availability of carefully prepared calcium buffer solutions (Molecular Probes, Eugene, OR).

Display and Analysis of Results

Analyses with fluo-3 require the observation of changing fluorescence intensities, while the analysis of indo-1 (and of fluo-3, if normalized for cellular loading differences by using the ratio to fluorescence of a second dye) requires determination of a ratio of two fluorescence intensities. Fortunately, commercial flow cytometers all have some provision for a direct calculation of the value of the fluorescence ratio, either by analog circuitry or by digital computation. If cellular indo-1 loading is extremely heterogeneous, it may be desirable to work with a logarithmic conversion of "violet" and "blue" emission intensities in order to observe a broader range of cellular fluorescence. In this case, the instrument must permit the logarithm of the ratio to be calculated by subtraction of the log "blue" from the log "violet" signals (10).

Plotted as a histogram of the ratio values, quiescent cell populations stained with indo-1 show narrow distributions of ration, even when cellular loading with indo-1 is very heterogeneous, and coefficients of variation (CVs) of less than 10% are common (Figs. 31.4*A* and 31.4*I*). For simple fluo-3 analyses, variation in dye loading will result in wider CVs (Figs. 31.4*B* and 31.4*J*). In either case, the effects of perturbation of $[Ca^{2+}]_i$ by agonists can be noted by changes in the histogram profiles, observed by storing histograms sequentially over time, with subsequent analysis of data.

A more informative and elegant display is obtained by a bivariate plot of indo-1 ratio or fluo-3 fluorescence intensity vs. time. The bivariate data can be displayed as "dot plots" on which the indo-1 ratio or fluo-3 intensity of each cell (proportional to $[Ca^{2+}]_i$) is plotted on the *Y*-axis vs. time on the *X*-axis (Figures 4*A* and 4*B*). Alternatively, the data can be presented as "isometric plots" in which the *X*-axis represents time, the *Y*-axis is indo-1 ratio or fluo-3 intensity, and the *Z*-axis is the number of cells (Figs. 31.4*K* and 31.4*L*). In these bivariate plots, kinetic changes in $[Ca^{2+}]_i$ are seen with much greater resolution, limited only by the number of channels on the time axis, the interval of time between each channel, and the rate of cell analysis. Changes in the fraction of cells responding, the mean magnitude of the response, and the heterogeneity of the responding populaiton are best observed with these displays. For example, it can be seen in Figures 31.4*A* and 31.4*K* that for $CD4^+$ T-cells at 1 min after the addition of antibody to CD3, the response is highly heterogeneous, with some cells not yet responding and other cells achieving very high levels of $[Ca^{2+}]_i$. Figures 31.4*B* and 31.4*L* show that when the analysis of fluo-3 and indo-1 in the same cells are compared, the presence of the broader CV of the measurement with fluo-3 results in a diminished ability to resolve the heterogeneity of the response.

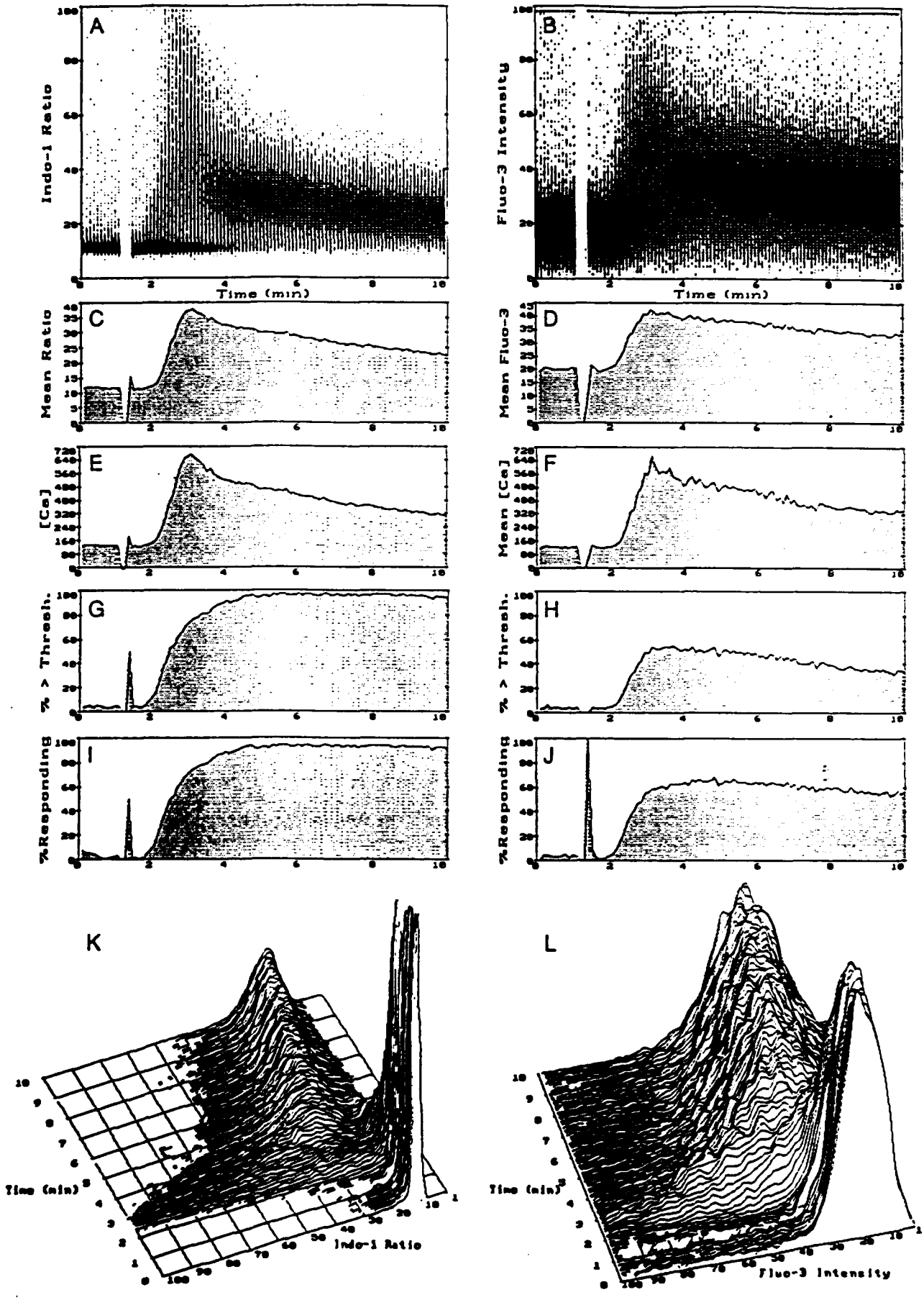

Figure 31.4. A-L

For many purposes, it is simpler and preferable to examine and compare a univariate parameter describing the cellular response vs. time. There are several such parameters that can be derived from the bivariate data for this purpose. Calculation of the mean *Y*-axis value for each *X*-axis time interval allows presentation of the data as mean ratio or fluorescence intensity vs. time (10), as shown in Figures 31.4*C* and 31.4*D*. Calibration of the ratio or intensity to $[Ca^{2+}]_i$ allows data presentation in the same manner as traditionally displayed by spectrofluorimetric analysis, i.e., mean $[Ca^{2+}]_i$ vs. time (Figs. 31.4*E* and 31.4*F*). While this presentation yields much of the information of interest in an easily displayed format, data relating to the heterogeneity of the $[Ca^{2+}]_i$ response are lost. Some of this information can be displayed by a calculation of the "proportion of responding cells." If a threshold value of the resting ratio distribution is chosen, i.e., one at which only 5% of control cells are above the threshold value, the proportion of cells responding by ratio elevations above this threshold vs. time yields a presentation that is informative of the heterogeneity of the response (Figs. 31.4*G* and 31.4*H*). A more sophisticated measure of the proportion of responding cells can be derived by the application of histogram subtraction techniques as illustrated in Figures 31.4*I* and 31.4*J*: The measurement of unperturbed cells in the initial period of observation can be used as the "control" fluorescence or ratio distribution; at each subsequent time interval, the cumulative subtraction technique (21) has been used to subtract the control distribution from the observed distribution. Comparison of Figure 31.4*H* with Figure 31.4*J* shows that the latter technique is less sensitive to the shape and width of the control distribution; this difference is more dramatic in Figure 31.5, described below.

Simultaneous Analysis of $[Ca^{2+}]_i$ and Other Fluorescence Parameters

The most common application for use of additional fluorochromes with $[Ca^{2+}]_i$ analysis will be the determination of cellular immunophenotype simultaneously with the $[Ca^{2+}]_i$ assay, allowing alterations in $[Ca^{2+}]_i$ to be examined in, and correlated with, specific immunophenotypic subsets. FITC- and PE-conjugated antibodies can be used with indo-1, and PE and allophycocyanine (APC) (or other red-excited dyes) can be used with fluo-3. Only the fluo-3/PE combination can be performed with a single-laser flow cytometer, the other combinations require a dual-laser flow cytometer.

Numerous examples of the analysis of $[Ca^{2+}]_i$ in immunophenotypically defined subsets have been described (review, 22). Several illustrative examples will demonstrate the utility of this approach. Figure 31.5 shows the simultaneous analysis of $CD4^+$ and $CD8^+$ subsets of PBL, performed using two-color immunofluorescence simultaneously with indo-1. This figure is also chosen in order to illustrate the importance of the interaction of receptors on the cell surface (in this case by cross-linking) and the relative contributions of internal and external calcium stores.

Addition of an anti-CD3 antibody alone (3 μg/ml, UCHT-1, Dako Corp) in this experiment had only a small effect upon $[Ca^{2+}]_i$ in either $CD4^+$ or $CD8^+$ subsets (see 2- to 4-min interval of Fig. 31.5). This antibody differs from that of Figure 31.4, in that the latter produces a greater $[Ca^{2+}]_i$ response in the absence of further cross-linking. When saturating amounts of goat antimouse antibody is added (at time 4 min), an intracellular calcium response is seen that is greater in $CD4^+$ cells than in $CD8^+$ cells. As the extracellular medium used in this experiment contained little Ca^{2+}, the response from 4 to 7.5 min represents mobilization from intracellular stores. This response is characteristically of short duration (compare Figs. 31.5*C* and 31.5*D* to Figures 31.4*E* and 31.4*F*), which is the strongest evidence that the extended phase of elevated $[Ca^{2+}]_i$ is maintained by influx of extracellular Ca^{2+}. To illustrate that calcium channels have, in fact, been opened by the cross-linked stimulus in Figure 31.5, Ca^{2+} was added to the extracellular medium at time 7.5 min; this is accompanied by an immediate elevation of $[Ca^{2+}]_i$, with a sustained response. Again, the magnitude of

Figure 31.4. Comparison of indo-1 and fluo-3 measurement of $[Ca^{2+}]_i$ and methods of displaying and analyzing calcium signaling in single cells as a function of time. Human PBL were loaded simultaneously with 3 μg/ml indo-1 and 3 μg/ml fluo-3, stained with PE-CD4 mAb, and then stimulated with anti-CD3 antibody (10 μg/ml G19-4, a gift from Dr. Jeff Ledbetter, Oncogen, Seattle, WA) at approximately 1 min after the start of analysis (note gap in data acquisition). Violet and green indo-1 emission (UV-excited) and green fluo-3 and orange PE emission (temporally delayed 488-nm excited) were collected simultaneously for each cell. Only results gated from $PE\text{-}CD4^+$ cells are displayed. In *A* and *B*, the results are displayed as a "dot plot" in which $[Ca^{2+}]_i$ is plotted for each cell analyzed on a 100 × 100 pixel grid, where the *X*-axis is time and the *Y*-axis is indo-1 ratio or fluo-3 fluorescence intensity. The number of cells per pixel is displayed by darkness that ranges over 12 levels. At the bottom, K and L, isometric plots of the same experiment in A are shown; sequential histograms are plotted in which the *X*-axis represents time, the *Y*-axis $[Ca^{2+}]_i$ or fluo-3 intensity, and the *Z*-axis number of cells. The mean indo-1 ratio vs. time is shown in C and fluo-3 intensity vs. time is shown in D. The data were converted to calcium concentration vs. time by calibration, using measured constants in equation 1 for indo-1 (E) and by calibration with buffer solutions for fluo-3 (F), and the values were plotted vs. time. Note that whereas the shapes of the curves for mean indo-1 ration (C) and fluo-3 intensity (D) are different (particularly in an apparently slower return to baseline after 4 min in (D), once converted to $[Ca^{2+}]_i$, the two measurements are essentially identical. The apparent discrepancy in C vs. D is related to the different values of Km for indo-1 and fluo-3. The percent cells responding with $[Ca^{2+}]_i$ elevated beyond two standard deviations above the mean of the cells before antibody stimulation ("percent cells above threshold") are plotted for indo-1 (G) and fluo-3 (H). The percent responding cells calculated by cumulative curve subtraction (see text) are plotted in I and J for indo-1 and fluo-3, respectively. Data analysis in this and subsequent figures was performed with a software program written by one of the authors (P.S. Rabinovitch) ("MultiTime," Phoenix Flow Systems, San Diego, CA).

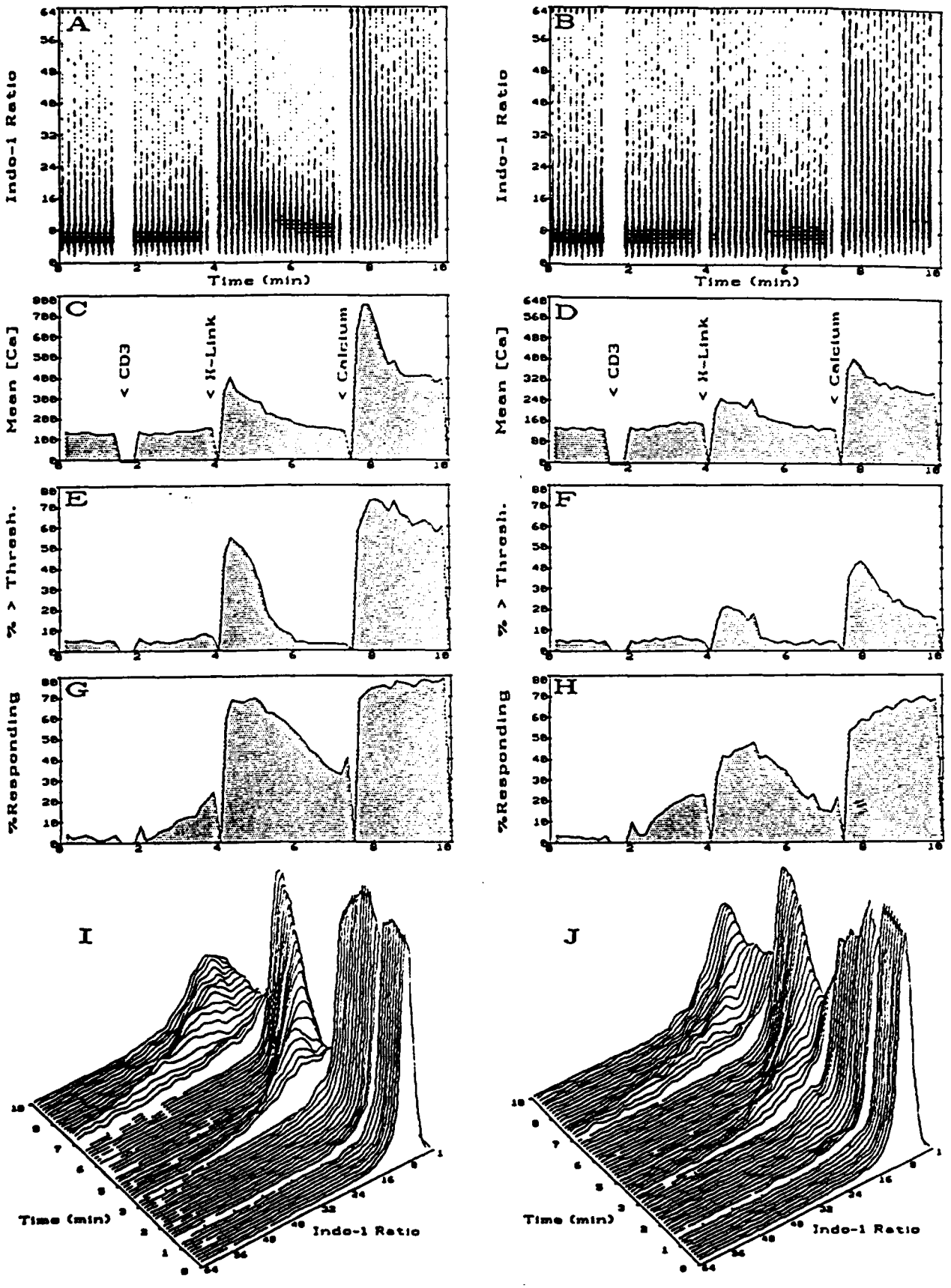

Figure 31.5. A-J

this final response is greater in $CD4^+$ cells than in $CD8^+$ cells.

Comparison of the percent of cells above a threshold (Figs 31.5*E* and 31.5*F*) with the proportion of responding cells calculated by curve subtraction (Figs. 31.5*G* and 31.5*H*) shows a substantial difference between the two measures: The latter calculation detects more responding cells than the former. This difference is greater in Figure 31.5 than in Figure 31.4, due in largest part to the presence in Figure 31.5 of a greater fraction of cells with elevated $[Ca^{2+}]_i$ in the "resting" control population; in such a case, a threshold set to exclude all but 5% of the "resting" population may be required to be at a relatively high $[Ca^{2+}]_i$ value, whereas the method of curve subtraction avoids this problem (21).

As a second example, Figure 31.6 shows the analysis of murine splenocytes. While approximately 50% of murine splenocytes are B-cells, only approximately 10% are T-cells (CD5-positive), as seen from the bivariate analysis of FITC-CD20 vs. PE-CD5 (Fig. 31.6*A*). When a T-cell stimulus (antibody to the T-cell receptor, CD3) is applied to the splenocytes, only a very small response is visible in the total population. In contrast, when the indo-1 analysis is gated upon the $CD5^+$ $CD20^-$ cells, then the response of the minority subpopulation of T-cells can be seen to be vigorous, and, as expected, the $CD5^-CD20^+$ cells show no response (Fig. 31.6*B*). Conversely, when a B-cell stimulus (anti-IgM) is applied, the response of the immunophenotypically identified B-cells shows twice the magnitude of that seen in the ungated total population of splenocytes, while the T-cell subset, as expected, shows no response (Fig. 31.6*C*).

Using other probes excited by visible light, it is possible to analyze additional physiologic responses in cells simultaneously with $[Ca^{2+}]_i$. The simultaneous analysis of membrane potential and $[Ca^{2+}]_i$ has been accomplished by several groups (23, 24), and simultaneous analysis of $[Ca^{2+}]_i$ and pH_i will be illustrated in a subsequent section of this chapter.

Sorting on the Basis of $[Ca^{2+}]_i$ Responses

The ability of the flow cytometric analysis with indo-1 to observe small proportions of cells with different $[Ca^{2+}]_i$ responses than the majority of cells suggests that the flow cytometer may be useful to identify and sort variants in the population for their subsequent biochemical analysis or growth. Results of artificial mixing experiments with Jurkat (T-cell) and K562 (myeloid cell) leukemia lines indicate that subpopulations of cells with variant $[Ca^{2+}]_i$ comprising <1% of total cells could be accurately identified (10). Goldsmith and Weiss (25, 26) have reported the use of sorting on the basis of indo-1 fluorescence to identify mutant Jurkat cells that fail to mobilize $[Ca^{2+}]_i$ in response to CD3 stimulus, in spite of the expression of structurally normal CD3/Ti complexes. These experiments suggest that sorting on the basis of indo-1 fluorescence can be an important tool for the selection and identification of genetic variants in the biochemical pathways leading to Ca^{2+} mobilization and cell growth and differentiation.

Critical Aspects in the Analysis of $[Ca^{2+}]_i$ by Flow Cytometry

COMPLICATIONS IN LOADING AND INTRACELLULAR ENVIRONMENT

Potential problems to be aware of in the use of $[Ca^{2+}]_i$ dye indicators include compartmentalization, leakage or secretion of dye, quenching by heavy metals, and incomplete deesterification of dye ester. The flow cytometric analysis of $[Ca^{2+}]_i$ using indicator dyes is predicated on achieving uniform distribution of the dye within the cytoplasm. In several cell types, the related dye fura-2 has been reported to be compartmentalized within organelles (27, 28). In bovine aortic endothelial cells, fura-2 has been reported to be localized to mitochondria; however, under those conditions, indo-1 remained diffusely cytoplasmic (29). Thus, it is possible that there will be fewer problems with compartmentalization of indo-1 than with fura-2. Some cell types, such as neutrophils and monocytes, and some cell lines (as opposed to primary cells) appear to be more susceptible to compartmentalization. In addition, compartmentalization is enhanced by prolonged incubation of cells at 37°C. In general, it is advisable to examine the cellular distribution of indo-1 or fluo-3 microscopically and, in each new application, to confirm the expected behavior of the dye. This is done by determining the ratio of R_{max} to R as a control for each experiment, as described below. In addition, one should store indo-1 loaded cells at room temperature after loading and use the cells promptly after loading. Since heavy metals may quench the

Figure 31.5. Analysis of $[Ca^{2+}]_i$ in human PBL stained with indo-1 and gated to show PE-positive CD4 cells (A, C, E, G, I) and PE-Texas-red-tandem-conjugate (ECD, Coulter Corp.) positive CD8 cells (B, D, F, H, J). Cells were suspended in medium with 5 mM EGTA, which reduced available extracellular Ca^{2+} to approximately 20 nM (10). At 1 min after the start of analysis, 3 μg/ml anti-CD3 mAb UCHT-1 was added (Dako Corp; this antibody by itself produces only a small $[Ca^{2+}]_i$ response), and at 4 min, 20 μg/ml goat antimouse antibody was added. The return to baseline after a brisk response is characteristic of mobilization of Ca^{2+} from intracellular stores, without influx of extracellular Ca^{2+} (see text). At 7 min, 10 mM $CaCl_2$ was added to the medium. A and B display "dot plots" of indo-1 ratio vs. time; C and D show calibrated $[Ca^{2+}]_i$ vs. time; E and F show the percent of cells above a threshold vs. time (the threshold ratio is set such that only 5% of "resting" cells are above that ratio, see text); G and H show the percent responding cells vs. time; and I and J show isometric displays of the indo-1 ratio vs. time.

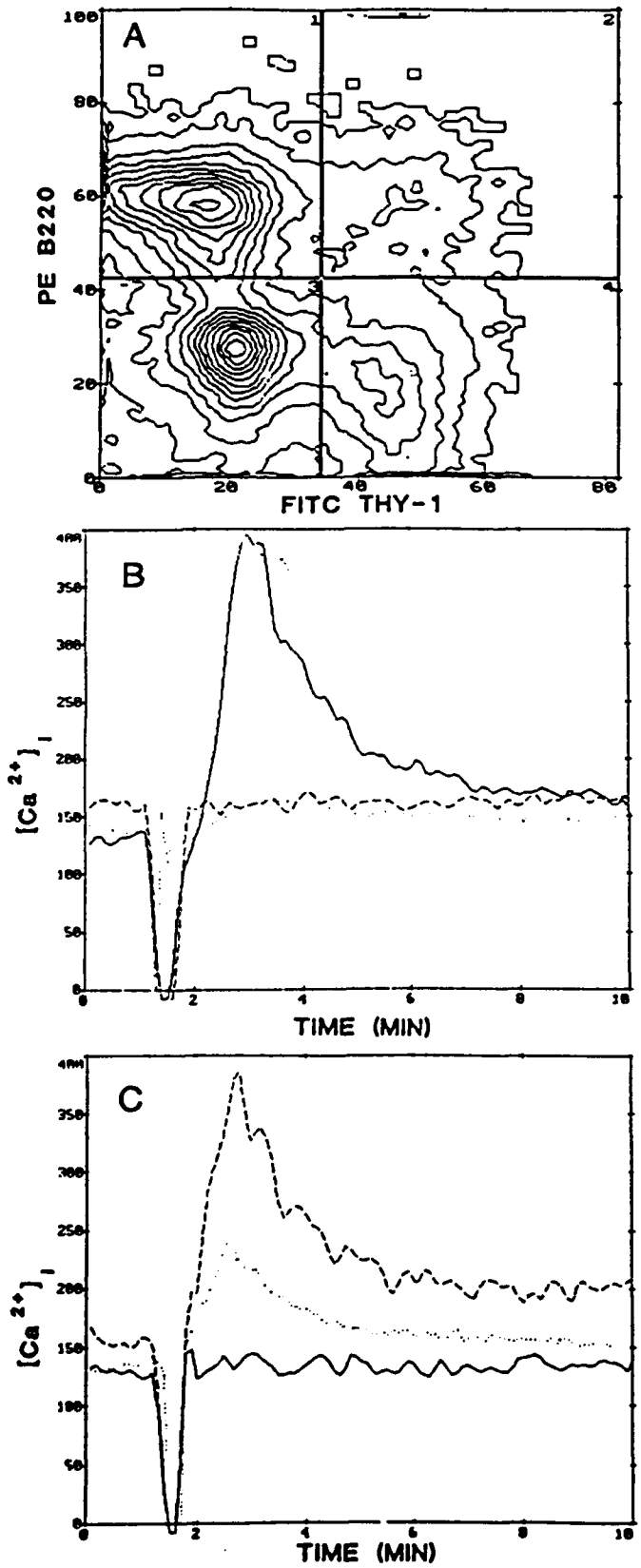

Figure 31.6. Analysis of splenic B- and T-cells. B6 mouse spleen cells were stained with PE-thy-1 (T-cells) and FITC B220 (B-cells). A shows the bivariate plot of FITC vs. PE. Fifteen percent of splenocytes are T-cells (*quadrant 4*) and 44% are B-cells (*quadrant 1*). B shows the result of stimulation with anti-CD3 mAb 2C11 (25 μg/ml). The ungated total cell response is small (*dotted line*), whereas the response gated upon the T-cell region of A is approximately sevenfold larger (*solid line*), and B-cells (*dashed line*) show no response. C shows stimulation with goat antimouse Ig (25 μg/ml): the response gated to show only B-cells (*dashed line*) is twice as large as that of all cells (*dotted line*) and T-cells (*solid line*) show no response.

indicator dye fluorescence, the use of the membrane permeant heavy metal chelator diethylenetriaminepentaacetic acid (TPEN) may be advisable for cell lines that contain increased amounts of heavy metals (30). In situations in which loaded dye is not retained intracellularly for a sufficient length of time, the dye is often being actively secreted and the use of probenecid, a blocker of organic anion transport, may be beneficial (27).

If, for a particular cell type loaded with indo-1, the magnitude of change between R and R_{max} is in good agreement with the values predicted from spectral curves of indo-1 in a cell-free buffer, then it would be unlikely that the dye is in a compartment inaccessible to cytoplasmic Ca^{2+}, in a form unresponsive to $[Ca^{2+}]_i$ (i.e., still esterified, see below), or in a cytoplasmic environment in which the spectral properties of the dye have been altered.

It has been suggested that both fura-2 and indo-1 (and by extension, presumably fluo-3) may be incompletely deesterified within some cell types (31, 32). Since the fluorescence of the ester has little spectral dependence upon changes in Ca^{2+}, the presence of this dye form could lead to false estimates of $[Ca^{2+}]_i$. Again, results of calibration experiments are helpful in excluding this possibility. Further, it has been proposed that since indo-1 fluorescence, but not that of the indo-1 ester, is quenched in the presence of mM concentrations of Mn^{2+}, then, in the presence of ionomycin, MN^{2+} can be used as a further test of complete hydrolysis of the indo-1 ester within cells (31).

Because of its more recent introduction, there is relatively little information available at this time regarding the relative importance of each of the above concerns when using fluo-3. To illustrate, however, the possibility that each dye may be subject to different intracellular processing and environments, Figure 31.7 shows results obtained with human peripheral blood lymphocytes (PBL) loaded simultaneously with indo-1 and fluo-3. Using UV and 488-nm excitation, each dye was independently but simultaneously analyzed in the same cells. After exposure to ionomycin, indo-1 showed the expected response associated with calcium influx; however, after an initial increase in fluorescence, fluo-3 intensity declined at the same time that the indo-1 ratio remained stably maximal. The reasons for the different behaviors of the two dyes is not yet clear, although it almost certainly is related to one or more of the points discussed above. This experiment demonstrates graphically the need

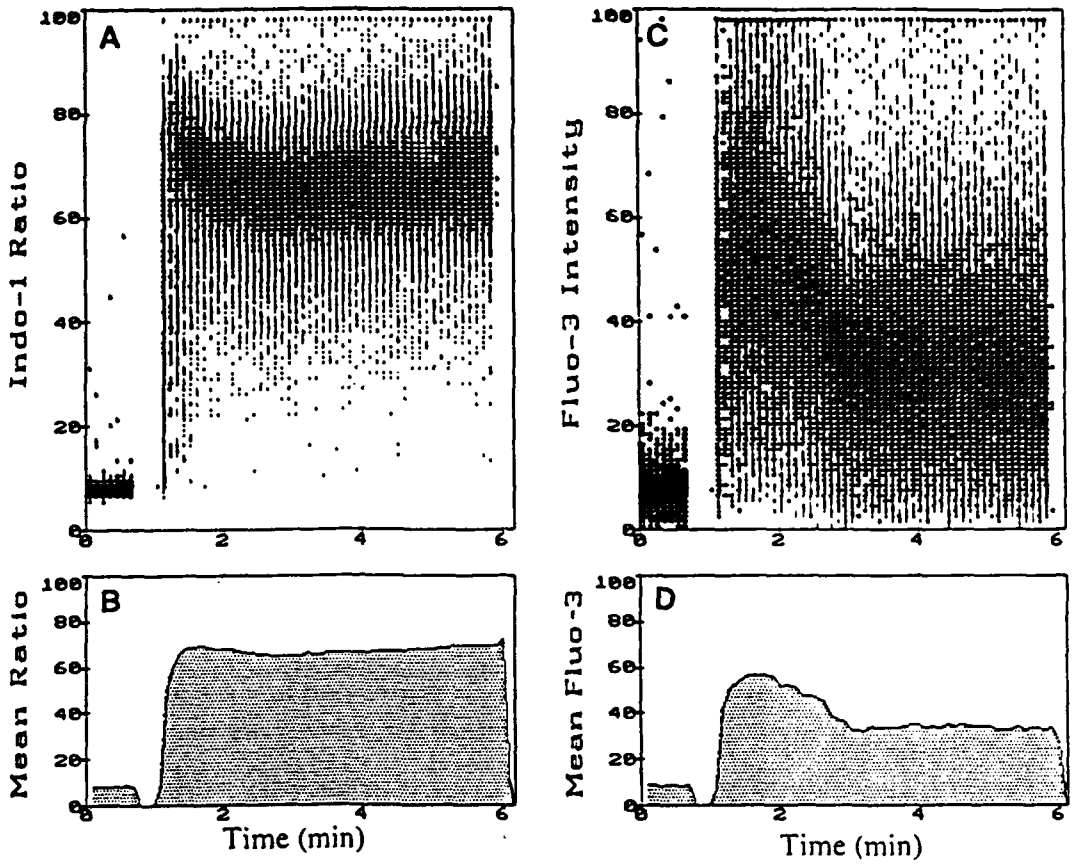

Figure 31.7. Ionomycin treatment of CD4+ peripheral blood T-cells simultaneously loaded with indo-1 and fluo-3. The indo-1 ratio is shown in A and B, and the fluo-3 intensity is shown in C and D. Note the partial return to baseline seen in fluo-3 intensity and not seen in the indo-1 ratio. This observation was variable over a series of experiments (data not shown).

for care in assessing correspondence to $[Ca^{2+}]_i$ by indicator dyes.

UNSTABLE OR BROAD BASELINE DISTRIBUTIONS

Under typical conditions, the baseline $[Ca^{2+}]_i$ distribution should show little (<3%) variation from sample to sample and should, with indo-1, be narrow and, most often, follow a normal (Gaussian) distribution. Some cell lines may have asymmetric distributions and altered mean values of "resting" $[Ca^{2+}]_i$, which can often be ascribed to a subpopulation of cells with elevated $[Ca^{2+}]_i$. This may result from the impaired viability of some cells, "spontaneous" activation of some subset of cells, or presumably, biological heterogeneity within the cell population (for example, cells within certain phases of the cell cycle). Sometimes, the baseline will start at a normal level and then rise with time. This may be due to the failure to completely remove from the sample lines an agonist from a previous experiment. The most common problem has been residual calcium ionophore; this can be efficiently removed by first washing the sample lines with DMSO and then scavenging residual ionophore by washing with a buffer containing 2% bovine serum albumin.

POOR CELLULAR RESPONSE

Failure of the cells to show proper response to various treatments may be due either to difficulty with the cells or with the instrument. To differentiate between these, the cells should be stimulated with the calcium ionophore ionomycin and the magnitude of R_{max} to R should be determined. If the indo-1 ratio of R_{max}/R increases by the amount described previously, or if the fluo-3 fluorescence increases by approximately five-fold, then the instrument is functioning properly. If the increase is less than expected, then one should obtain an independent preparation of cells, such as murine thymocytes or human PBL. If these cells load properly and also respond poorly, then the instrument alignment should be checked. With indo-1, not uncommonly, the violet or blue signals may not be properly focused, or there might be interference from a second laser. This problem can be pinpointed by analyzing separately the blue and violet signals after io-

nophore treatment; the violet signal should increase approximately threefold and the blue signal should decrease approximatley twofold (Fig. 31.2).

If the instrument is functioning properly, then the problem may be in the cells. The cells must be loaded with sufficient indo-1 or fluo-3 to be detectable well above autofluorescence. If there is any question, this should be checked independently with fluorescence microscopy, especially if one has become familiar with the expected fluorescence of loaded cells examined in this manner. If the cells are too dim or excessively bright or if the dye is compartmentalized, the ability to detect calcium signals will be impaired. For unknown reasons, the calcium signaling of B-cells, and not T-cells, is particularly sensitive to overloading with indo-1 (10, 13). The cells must be suspended in media that contains calcium; occasionally, responses will appear blunted because of the inadvertent resuspension of cells in a medium than contains no added calcium.

EFFECT OF ANTIBODY LABELING

In the simultaneous analysis of $[Ca^{2+}]_i$ and immunofluorescence, consider that the use of the antibody probe can itself alter the cellular $[Ca^{2+}]_i$. It is becoming increasingly clear that the binding of monoclonal antibodies (mAbs) to cell surface proteins can alter $[Ca^{2+}]_i$, even when these proteins are not previously recognized as part of a signal transducing pathway (10, 33–38). For example, antibody binding to CD4 will reduce CD3-mediated $[Ca^{2+}]_i$ signals; if the anti-CD4 mAb is cross-linked to the CD3 complex, as with a goat–antimouse mAb, the CD3 signals are augmented (39, 40). Antibody binding to CD8 has similar effects (unpublished data).

As a consequence of these concerns, a reciprocal staining strategy should be used whenever possible so that the cellular subpopulation of interest is unlabeled while undesired cell subsets are identified by mAb staining. The $CD4^+$ subset in PBL may be identified, for example, by staining with a combination of CD8, CD20, and CD11 mAbs (10), and the $CD5^+$ subset can be identified by staining with CD16, CD20, and HLA-DR mAbs (35). Finally, it is important to reiterate that, when staining cells with mAbs for functional studies, antibodies must be azide-free for metabolic processes to be uninhibited. Commercial antibody preparations may thus require dialysis before use.

INTRINSIC LIMITATIONS OF FLOW CYTOMETRY

Flow cytometry is unable to detect heterogeneity of cellular calcium concentrations within a single cell, and there are reports from assays using digital video microscopy that, in some situations, calcium transients may be present only within compartmentalized sublocations (41, 42). It has been reported that the photoprotein aequorin may in some circumstances help to detect changes in cytosolic calcium not reported by indo-1 (43), although use of the two indicators is complementary because aequorin cannot measure Ca^{2+} in single cells (44). In addition, there is evidence that calcium elevations occurring after cellular stimulation may be oscillatory rather than sustained (45, 46), thus raising the possibility that some cellular processes controlled by calcium may be frequency-modulated as well as amplitude-modulated. Since flow cytometry cannot measure the calcium concentration inside a single cell as a function of time, it is not possible to distinguish whether there is a subpopulation of cells that is responding with a sustained response or, alternatively, whether there are two populations of cells, one that has elevated calcium concentration and one that has basal levels. In spite of these limitations, determination of $[Ca^{2+}]_i$ in large numbers of single cells using flow cytometry with indo-1 offers great practical advantages and allows measurements of a kind that is not possible to achieve by means of the alternative techniques that are currently available.

Applications of the Flow Cytometric Analysis of $[Ca^{2+}]_i$

The flow cytometric assay of cellular calcium concentration has already been applied to a wide variety of cells, providing interesting and sometimes unexpected results. Examples of the initial applications of the technique are presented in recent reviews (47, 48). One of the first observations that was made readily quantifiable by the flow cytometric analysis was that there is great heterogeneity in the response of lymphocytes to mitogenic agonists. Using simultaneous immunofluorescence, some of this heterogeneity can be shown to be related to immunophenotypic subsets; for instance, $CD4^+$ cells show more vigorous responses to phytohemagglutinin, concanavalin A, and mAb to CD3 (see Fig. 31.5) than do $CD8^+$ cells (10, 49). Considerable use of this approach has been made in the demonstration of differences between $[Ca^{2+}]_i$ activation requirements of different cell subsets and subset specificities of activation pathways. The effects of antibody binding to cell surface molecules, sometimes a complication in labeling experiments (see above), has been extensively employed to analyze signaling mechanisms, and augmented, or even new relationships have been probed by cross-linking antibodies on the cell surface (39, 50). Flow cytometric measurements with indo-1 have been performed to date with all nucleated blood cell types. Applications of fluo-3 have been reported with most types, with reports appearing at a rapidly increasing pace. The combination of sensitivity, reliability, and ability to analyze large numbers of cells within cell subsets has made the flow cytometric assay of $[Ca^{2+}]_i$ the preferred technique for a broad spectrum of research applications.

There are many potentially exciting clinical applications of the flow cytometric assay of cellular calcium concentration (47). One topical example is the study of the effects of the human immunodeficiency virus (HIV) infection. In in vitro studies, the HIV-1 retrovirus was found to impair signal

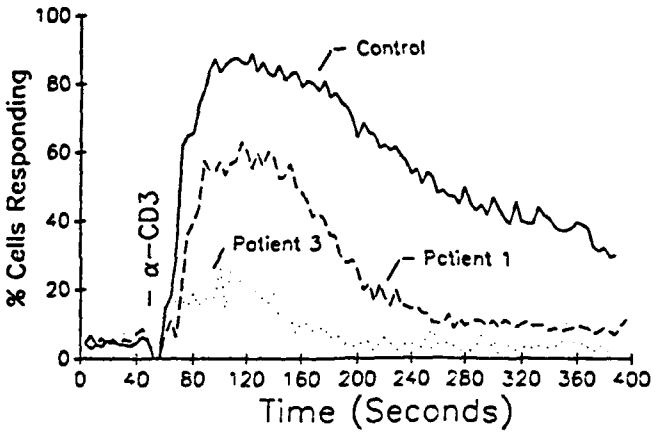

Figure 31.8. PBL from asymptomatic HIV-infected patients or an uninfected control donor were stained with FITC-CD8 and PE-CD5. The cells were loaded with indo-1, stimulated with anti-CD3 antibody 38.1 (1 μg/ml), and changes in calcium were monitored in the $CD4^+$ ($CD5^+CD8^-$) cells. The time course of the percent of responding cells is shown.

transduction in CD4 cells, the major target of HIV-1 (51). Recent studies suggest that CD4 T-cells from HIV-infected patients also have impaired responses to T-cell receptor stimulation (G.P. Linette et al., unpublished). Due to the necessity of analyzing live, retrovirus-infected cells on the flow cytometer, a closed fluidics system is used to prevent the generation of aerosols. Lymphocytes from patients with early-stage HIV infection (Walter Reed stage II-III) have been isolated, loaded with indo-1, and the CD4 subset has been analyzed by gating on the $CD5^{bright+}$ $CD8^-$ subset of cells. More than 80% of HIV-infected patients have anti-CD3-induced calcium responses that are below that of age- and sex-matched control donors. There is substantial patient-to-patient variability, with some patients having minimally diminished responses and others displaying severely reduced signaling (Fig. 31.8). Thus, both normal CD4 T-cells after HIV infection in vitro, and the CD4 T-cells from patients with early stage HIV infection have impaired signal transduction. It is likely that the mechanism of impaired signaling may differ in vitro vs. in vivo. During in vitro infections, more than 50% of the CD4 cells can be shown to be infected. In contrast, <1% of CD4 cells from patients with early-stage HIV infection can be demonstrated to be infected, so that an indirect mechanism must exist for the virus to impair signal transduction pathways in uninfected cells. In any case, the existence of this abnormality may prove to be a sensitive test of the immune system function in HIV infections. Current studies in several laboratories are exploring whether or not this application may provide prognostic information and whether the assay may be useful for the management of this chronic illness. Study of HIV infection does illustrate the utility of flow cytometry in the clinical setting in which only one immunological subset of cells, or a portion of cells, in that subset may show an altered response. Demonstration of such heterogeneity in $[Ca^{2+}]_i$ signals would have been impossible to discern in conventional assays carried out in a fluorimeter where only the mean calcium response is recorded.

INTRACELLULAR pH

Introduction

The pH_i of mammalian cells is ~7.2, and pH_i appears to be closely regulated (the coefficient of variation measured by flow cytometry is ~5%). In mammalian cells, pH_i is regulated by at least three mechanisms, including Na^+_o/H^+_i exchange, sodium-dependent $Cl^-_o/HCO_{(3)}^-{}_i$, and $HCO_{(3)}^-{}_o/Cl^-_i$ exchange. Acid extrusion is primarily accomplished by the Na^+/H^+ antiport and by sodium-dependent $Cl^-_o/HCO_{(3)}^-{}_i$, while $HCO_{(3)}^-{}_o/Cl^-_i$ exchange has the major role for base extrusion. All of these mechanisms appear to be stimulated by a variety of growth factors and by phorbol esters, presumably through the activation of protein kinase C. It was initially proposed that an alkaline shift in pH_i itself might be a signal to regulate cell activation. A number of reports purporting to show a role for pH_i in cellular activation are derived from measurements made in bicarbonate-free medium. Thus, nonphysiologic ($HCO_{(3)}$-free) buffers were used so that only the Na^+/H^+ antiporter could operate and, thus, alkalinization was the dominant response. Recent reports, performed in physiologic medium, show that cellular activation is, in fact, accompanied by acidification in many cases and that the net effect (acidification or alkalinization) is a function of the medium in which the experiment is conducted. Thus studies of pH_i are important physiologic tools for the elucidation of various ion exchange mechanisms but cannot be taken as evidence per se of cellular activation (52).

Indicators of Intracellular pH

Until recently, the most commonly used probes were modifications of fluorescein—fluorescein diacetate being the first-generation pH probe—followed by carboxyfluorescein diacetate (COFDA). Both of these dyes are limited by relatively poor retention inside loaded cells. An improved fluorescein probe is 2′,7′-bis-carboxyethyl-5(6)-carboxyfluorescein (BCECF). As with indo-1 and fluo-3, BCECF is loaded into cells using the acetoxymethyl ester; after hydrolysis, it has a negative charge of −4 or −5 and, therefore, leaks more slowly than COFDA. The pKa of BCECF, 6.98, is near the pH_i of resting cells, and there is a pH-dependent shift in the excitation wavelength, making it possible to use the ratio of fluorescence signals to correct for differences in loading and cell size. In addition, BCECF fluorescence excited at 450 nm is pH-independent, while fluorescence at 500 nm is pH-dependent, allowing ratiometric fluorescence

Table 31.1
Fluorochromes for Ratiometric Determination of pH Using Flow Cytometry

Probe +	pKa	Fluorescence (nm) Excitation	Emission	References
Bis-carboxyethyl-carboxyfluorescein	6.98	ratio 439/490	535	Paradiso et al. (130)
Acetoxymethyl ester (BCECF AM)		488	ratio 520/620	Musgrove et al. (131)
Diacetoxy-dicyanobenzene (ADB); yields Dicyanhydroquinone (DCH) after de-esterification	8.0	~350	ratio 425/540	Cook and Fox (132) Musgrove et al. (131)
Carboxy SNARF-1 acetoxymethyl acetate (SNARF-1)	7.50	514 or 530	ratio 575/670	Whitaker et al. (55)

emission analysis (Table 31.1). In both cases, the magnitude of pH-dependent ratio shifts is relatively modest (for example, when the pH is raised from 6.5 to 7.5, the ratio of fluorescence intensities after excitation of FDA at 436 nm and 495 nm increases by only 1.45 to 1.55 times (53)); this is much less of a shift than is seen with SNARF-1 (see below) and, thus, these dyes are largely supplanted by the latter.

Subsequently, several UV-excited pH probes were developed. The most useful of these is 1,4-diacetoxy-2,3-dicyanobenzene (ADB). The cell-permeant ADB is hydrolyzed and trapped intracellularly to yield 2,3-dicyanohydroquinone (DCH) (54). DCH fluorescence is pH-dependent, while the esterified forms exhibit pH-independent fluorescence; therefore, care must exercised to ensure complete deesterification of the ADB. Ratiometric determinations of pH are possible using a single excitation source by measuring fluorescence emission at 429 nm and 477 nm (Table 31.1). As with measurement of $[Ca^{2+}]_i$, many laboratories will find the requirement for UV excitation to be the primary limitation for use of this probe.

Recently, the most useful probe for pH_i measurement has been introduced; a compound termed SNARF-1 (SemiNaphthoRhodaFluor) (55). This is the first pH probe to have fluorescence characteristics that provide truly useful and sensitive ratiometric properties. SNARF-1 appears to be the most promising reagent for use in flow cytometry, as it has convenient excitation spectra and exhibits large changes in pH-dependent fluorescence (Fig. 31.9). The acid form of SNARF-1 has absorption maxima at 518 and 548 nm, while the base form excites maximally at 574 nm. The emission of SNARF-1 in acid is maximal at 587 nm and the basic form emits maximally at 636 nm; there is an isosbestic point at 610 nm. In practice, either the 530-nm line of a krypton-ion laser or the 514-nm line of an argon-ion laser are optimal for excitation, while emission should be collected at both 575 nm and 640 nm and the ratio of these signals calculated. Excitation of SNARF-1 at 488 nm is only slightly less optimal; because it has the advantage of permitting simultaneous analysis of FITC probes (i.e., immunofluorescence), this will probably be the most commonly used excitation wavelength.

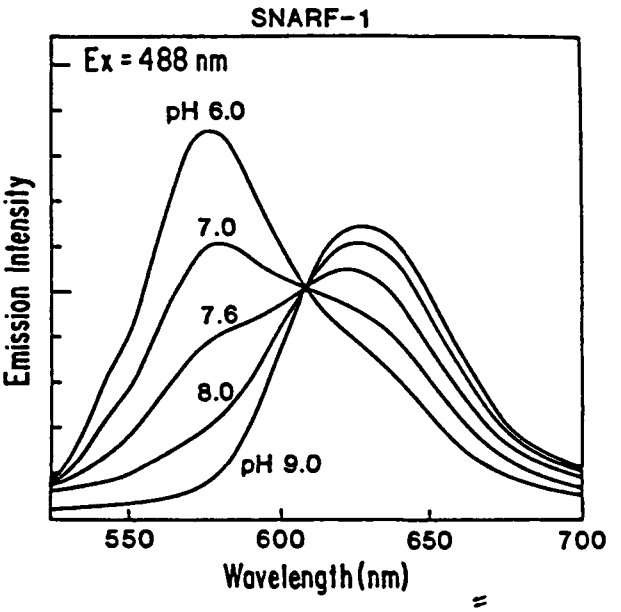

Figure 31.9. Fluorescence emission spectra of SNARF-1 as a function of pH. Excitation was at 488 nm. (Courtesy of R. Haughland, Molecular Probes, Eugene, OR).

Preparation of Cells for SNARF-1 Analysis

As with indo-1, the optimal conditions for loading must be empirically determined for each cell type. Cells must be loaded only to the point where the fluorescence signal is above autofluorescence and sufficient for detection by the flow cytometer. A typical loading protocol is:

1. Incubate cells ($\leq 2 \times 10^7$/ml) in buffered (for example, HEPES (4-(2-hydroxyethyl)-1-piperazine-ethanesulfonic acid), see above for rationale for using bicarbonate-free buffer or not) medium with 2–6 μM carboxy SNARF-1 (diacetate) at 30°C to 37°C for 30 min.
2. Centrifuge and resuspend in fresh medium at the desired cell concentration (usually ~10^6/ml). Store cells at 22°C and protect from light until analysis. The cell pellet will appear faintly pink.
3. Warm aliquot of SNARF-1 loaded cells to 37°C for 5 to 10 min before analysis. The medium and sheath fluid should be buffered saline. The rate of cell analysis can vary; commonly, cells are analyzed at 200 to 300 cells/sec.

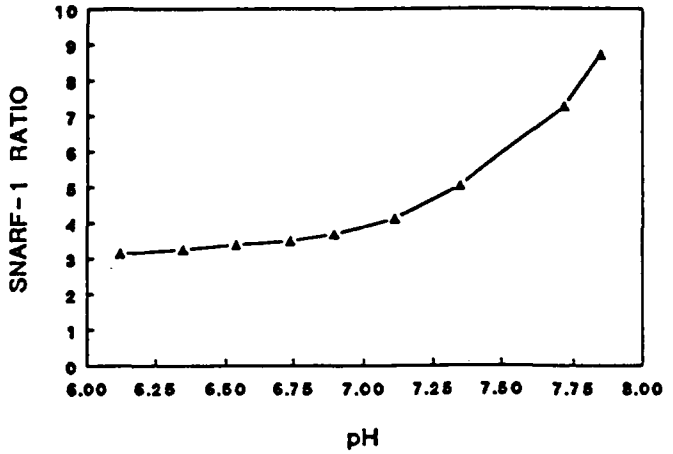

Figure 31.10. Calibration of the SNARF-1 ratio of fluorescence (670/575 nm) to pH. Jurkat cells were loaded with SNARF-1 and resuspended at 37°C in buffers containing 135 nM K^+ with varying pH in the presence of nigericin. Excitation was at 514 nm.

Flow Cytometric Analysis of SNARF-1-Loaded Cells

As described above, SNARF-1 emission should be collected using orange and red bandpass filters centered at 570 nm (orange) and 640 to 670 nm (red). The ratio of red/orange fluorescence intensity is proportional to increasing pH (Fig. 31.10). See the corresponding section above on indo-1 analyses for further discussion of ratiometric analysis.

SNARF-1 is a vital dye and, therefore, dead cells are efficiently excluded from analysis by electronically gating on cells that have fluorescence. If FITC fluorescence is measured simultaneously, as for determination of cell subsets, suitable gating on this parameter would also be used. Using single-beam 488-nm illumination for analysis of FITC fluorescence requires compensation for overlap into the green FITC bandpass from the leftward tail of the SNARF-1 emission spectrum. This is analogous to the routine color compensation used when analyzing PE with FITC, except that even greater crossover compensation may be required when the SNARF-1 fluorescence is bright. Alternatively, cells can be stained with amino-methycoumarin acetic acid (AMCA)-conjugated antibodies and fluorescence analyzed using UV illumination, thereby avoiding the need for compensation.

The effective Kd of SNARF-1 for protons is 7.5, which is near the pH_i of resting cells (pH_i = ~7.2). The pH_i of stimulated cells may decrease or increase, depending on cell type, stimulus, and medium composition (52). As seen in Fig. 31.9, described below, SNARF-1 has a greater sensitivity in reporting alkaline shifts than acidification.

Calibration and Data Analysis

For each experiment, it is necessary to construct a calibration curve so that one may determine the fluorescence channel number as a function of pH_i. Cells are suspended in a series of high potassium buffers of different pH (with otherwise identical ionic composition). The cells should be loaded with the pH probe and treated with the proton ionophore nigericin (1 μg/ml), added in order to equalize pH_i and to buffer pH (56). Nigericin produces the equilibrium $[K^+_i]/[K^+_e] = [H^+_i]/[H^+_e]$. Thus, in the presence of nigericin, pH_i can be calculated with the knowledge of $[K^+_i]$, $[K^+_e]$ and the buffer pH. Equilibrate tube at 37°C for 15 min, and measure SNARF-1 fluorescence ratio at 37°C. Note that nigericin is toxic to human lymphocytes at >5 μg/ml, manifested by loss of cellular fluorescence.

A calibration curve can be constructed by plotting values of pH_i vs. the SNARF-1 fluorescence ratio (Fig. 31.10). The ratio changes ~3-fold between pH 6.0 and pH 8.0. Most of the ratio shift occurs between pH 7 and pH 8, as the slope of the curve is much less between pH 6 and pH 7.

Simultaneous Analysis of pH and Other Fluorescence Parameters

As mentioned above, the fluorescence emission properties of SNARF-1 allow simultaneous excitation of FITC probes using the same 488-nm laser. Analysis of pH_i in immunophenotypically-defined cell subsets using FITC-conjugated mAb is thus very straightforward. Similarly, single-laser $[Ca^{2+}]_i$ measurements with fluo-3 simultaneously with pH_i are easily performed. When a second UV laser is available, $[Ca^{2+}]_i$ measurement with indo-1 is preferred. Fig. 31.11 illustrates the analysis of $[Ca^{2+}]_i$ and pH_i in splenic T-cells. FITC-CD4 mAb was used to gate the analysis specifically upon this subset of murine splenocytes (not shown), and the ratios of UV-excited green and violet indo-1 emission and 488-nm-excited red and orange SNARF-1 emission were each calculated. The elevation in $[Ca^{2+}]_i$ reached its peak within 5 min after antibody to the T-cell receptor (CD3) was added and, subsequently, slowly declined (Fig. 31.11*A*). Intracellular pH_i reached its peak more slowly, 10 min after addition (a 0.2 unit alkalinization), and thereafter also slowly declined toward baseline (Fig. 31.10*B*).

INTRACELLULAR GLUTATHIONE

Introduction

Glutathione (glutamylcysteinylglycine, GSH) is an important antioxidant tripeptide thiol that is involved in the scavenging of toxic oxygen products (57–59). In addition, GSH is involved in a number of other important reactions in the cell, including conjugation of xenobiotics, amino acid transport, and deoxyribonucleotide synthesis (57). GSH is also important for the maintenance of cellular thiol redox status, and its redox state has been proposed to be a major determinant of the functioning of a number of enzymes (60–66) and of the integrity of cytoskeletal proteins (67). The biochemical pathways of GSH synthesis, renewal, and utilization are outlined in Fig. 31.12.

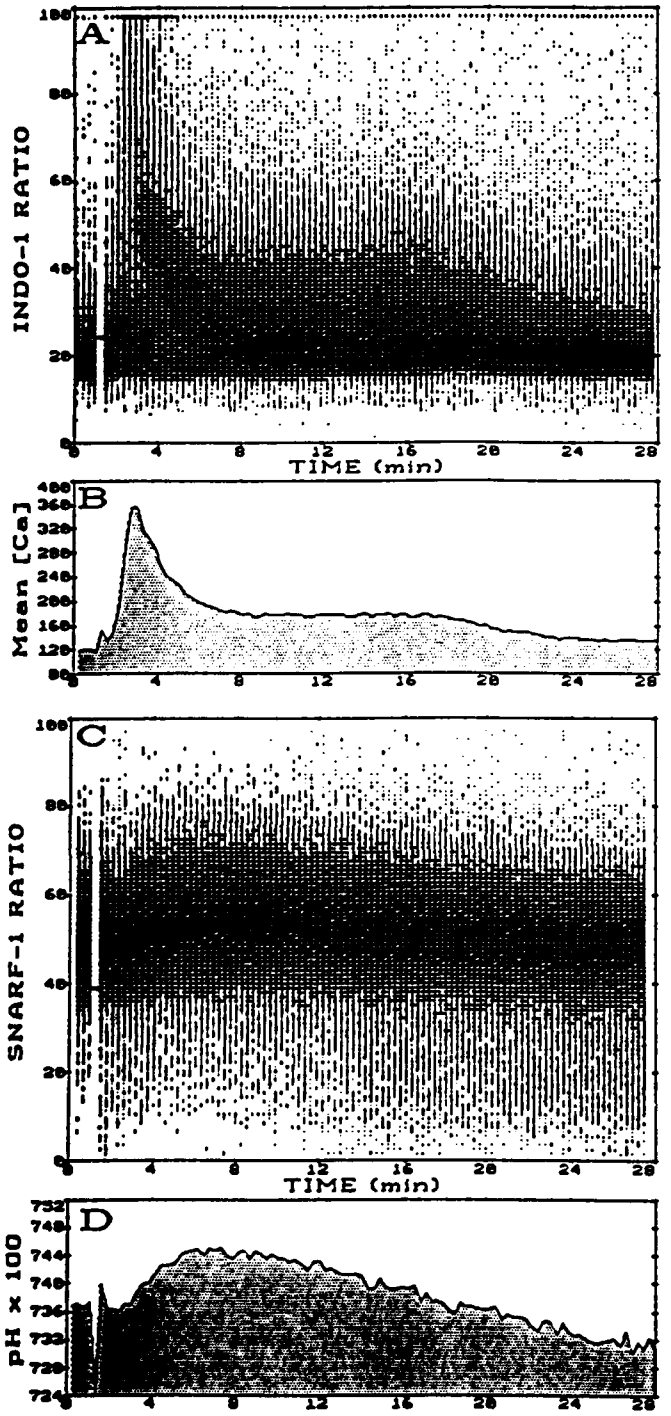

Figure 31.11. Simultaneous analysis of murine splenocytes loaded with indo-1 and carboxy SNARF-1. Murine splenocytes were loaded with indo-1 and SNARF-1 and stained with FITC-conjugated anti-CD4 mAb. Fluorescence was excited by the UV lines of a krypton-ion laser and the 488-nm line from an argon-ion laser. The ratio of indo-1 fluorescence (395 nm/525 nm) and of SNARF-1 fluorescence (665 nm/575 nm) is displayed vs. time. The analysis was gated on the FITC-CD4 fluorescence at 525 nm. Anti-CD3 antibody 2C11 was added during the gap in the analysis. The calcium and pH values for individual cells are plotted as dot plots in the upper panels, and the mean response vs. time is plotted in the lower panels. $[Ca^{2+}]_i$ increased from 0.13 μM to 0.36 μM and pH, increased 0.2 units.

These roles for GSH have important consequences upon cell physiology and mitogenic activation. In general, augmenting cellular GSH with cysteine delivery agents such as *N*-acetycysteine, oxathiayolidine carboxylic acid, or glutathione esters has a positive effect on cell growth, whereas depletion of GSH inhibits many cellular functions (57). GSH is known to influence cell growth and replication at various levels including G_1/S-phase transition (68, 69) and very early events in mitogen-induced cell activation (70). We will discuss later in this chapter some evidence that GSH affects very early steps of signal transduction. Other aspects of cell growth, such as protein synthesis, are also influenced by GSH levels, since γ-glutamyl transferase-dependent amino acid transport utilizes GSH (71). Interestingly, although activation steps that are important for cell replication of lymphocytes are GSH-dependent, those activation steps that are necessary for acquisition of differentiated functions are not necessarily GSH-dependent (72), although some workers have reported that GSH content can influence these functions as well (73, 74).

GSH has also been shown to affect the responsiveness of cells to various cytokines. For example, intracellular GSH has been shown to enhance the action of IL-2 in lymphocytes (72, 73, 75, 76), whereas extracellular GSH has been shown to decrease the effects of granulocyte/macrophage colony stimulating factor (GM-CSF) and platelet-derived growth factor (PDGF) on granulopoiesis and fibroblast proliferation, respectively (77, 78). For GM-CSF, this effect is thought to be mediated through direct competition by GSH for the GM-CSF receptor. In fact, GSSG, the oxidized form of GSH was found to have the capacity to stimulate the GM-CSF receptor directly (78). The mechanisms responsible for the inhibitory effects of GSH on PDGF-stimulated fibroblast growth are less well understood.

The activity of redox-responsive oncogene products and DNA-binding factors responsible for gene regulation may also be affected by the GSH status of the cell (79–85). For instance, the interaction of c-*fos* and c-*jun* products are known to be redox-sensitive (79). Another example is that of NFkB. Roederer and colleagues (83) have shown that this nuclear binding factor can be inhibited from binding to regulatory DNA binding domains by *n*-acetylcysteine, a drug that increases the GSH level of cells.

Finally, GSH has recently received attention because of its role in a number of pathological disease states, including tumor cell resistance to chemotherapeutic agents (98, Chapters 14 and 27, this volume), idiopathic pulmonary fibrosis (86, 87), and acquired immune deficiency syndrome (83, 88–91).

Fluorescent Indicators of Intracellular GSH

Several years ago Durand and Olive (92) published a review of fluorescent indicators for thiols, including GSH, that might prove useful for flow cytometric purposes. The prob-

OVERVIEW OF GLUTATHIONE METABOLISM

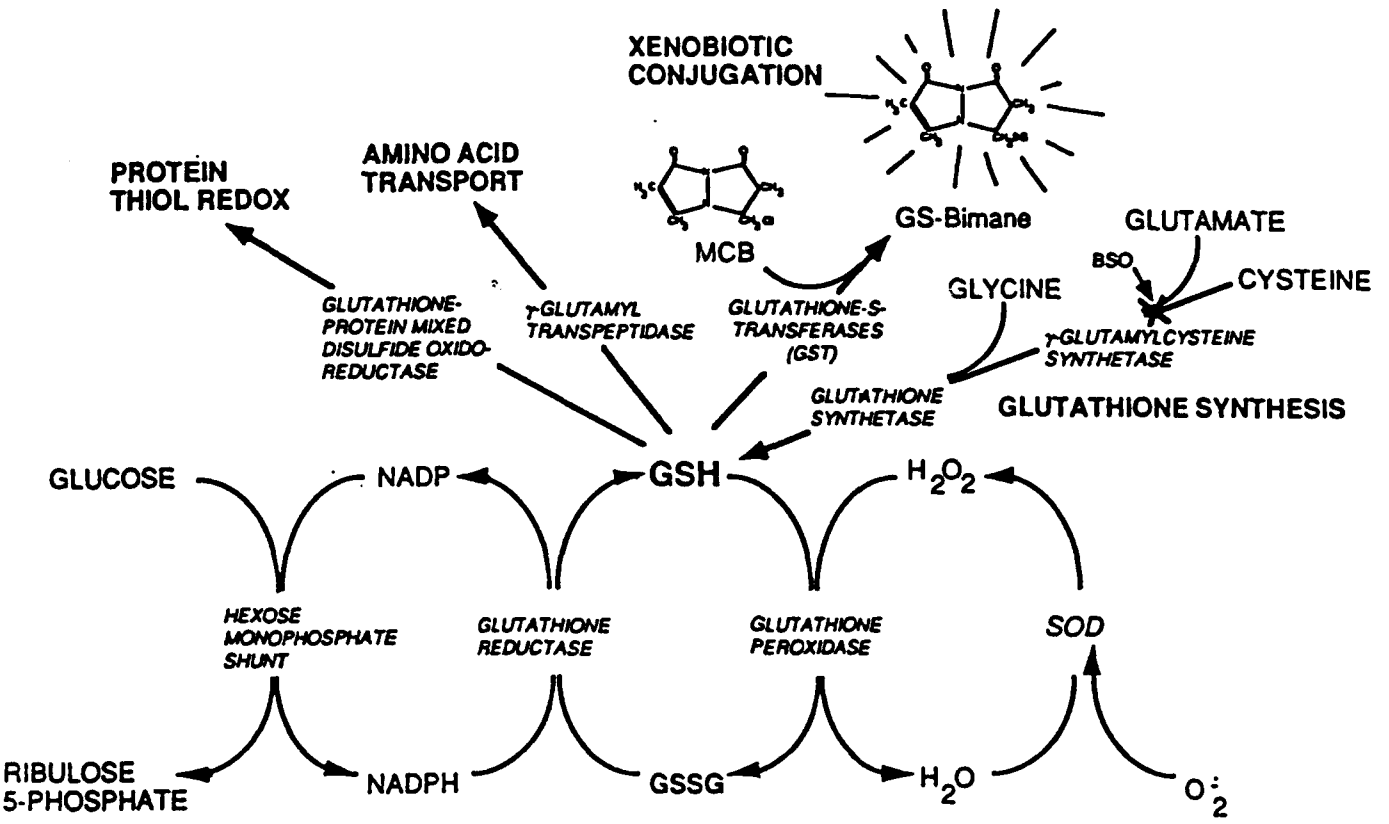

Figure 31.12. Overview of glutathione (*GSH*) metabolism. *GSH* is synthesized in a two-step process (upper right hand portion of figure): cysteine is metabolized to *g*-glutamylcysteine (*g*-CC) by *g*-GC synthetase and then to *GSH* by *GSH* synthetase. In the glutathione redox cycle (lower portion of figure) glutathione peroxidase uses *GSH* to reduce hydrogen peroxide and other peroxides and, in the process, *GSH* becomes oxidized (*GSSG*). Reduction of *GSSG* to *GSH* by glutathione reductase requires *NADPH*, supplied primarily by the hexose monophosphate shunt (also called the pentose phosphate shunt). *GSH* can also serve as a cosubstrate for glutathione transferase-mediated conjugation of xenobiotics (shown here is the conjugation of monochlorobimane (*MCB*), to the fluorescent glutathione-bimane conjugate, top of figure). *GSH* also has important roles in amino acid transport and in the maintenance of protein thiol redox status (upper left of figure).

lem with all of the dyes reviewed was one of specificity for GSH. Durand and Olive (92) concluded that a promising reagent at the time for flow cytometric determination of GSH was monobromobimane (MBB). Poot et al. (93) used this reagent in their investigation of human diploid fibroblast GSH metabolism, and employed *n*-ethylmaleimide-treated "blanks" in order to control for nonspecific protein thiol binding.

Another reagent that has since been introduced for flow cytometric evaluation of GSH is o-phthaldialdehyde (OPT) (94). OPT is supposedly more specific for GSH than MBB because, in addition to reacting with the cysteine thiol group of GSH, it also reacts with the amino terminus of GSH, forming a highly fluorescent cyclic structure. However, this dye has the same disadvantage as MBB of potentially binding to other nonprotein thiols in the cells such as cysteine and γ-glutamylcysteine. Nonetheless, OPT still has the advantage that, when bound to protein thiols, it has slightly different spectral characteristics than when bound to GSH (higher blue fluorescence and less green fluorescence), allowing one to simultaneously measure the sulfhydryl redox status of protein and of low molecular weight thiols (94).

A major advance in the measurement of GSH by flow cytometry was made by Rice et al. (95), who used monochlorobimane (MCB) to detect changes in GSH status of individual normal and tumor cells. Many papers have since been published applying this technique to a number of interesting problems in biology and medicine (70, 96–102). This

dye owes its specificity for GSH to the fact that it is conjugated to GSH by glutathione-S-transferases (GSTs) (see below) and has relatively low nonenzymatic reactivity toward GSH and other thiols (103).

Another reagent, chloromethylfluorescein diacetate (CMFDA) has recently been described for measuring intracellular GSH (104). Once inside the cell, this dye is deesterified to a hydrophilic cell impermeant product chloromethylfluorescein (CMF) by nonspecific esterases. CMF is then presumably metabolized in a manner similar to MCB, yielding a GSH-MF fluorescent conjugate. The advantage provided by this dye is that excitation and emission characteristics are similar to fluorescein once conjugated to GSH, allowing one to use this dye simultaneously with UV excitable dyes—for instance, with Hoechst 33342 for simultaneous GSH and DNA determinations (see below). The principal disadvantage of this dye is that it is apparently less specific for GSH than MCB (104).

Performing and Calibrating GSH Analysis

FACTORS THAT AFFECT THE UTILITY OF MCB FOR GSH MEASUREMENTS

We and others have found that the conditions required to adequately stain cells for GSH content with MCB depend upon several factors, including the concentration of dye used, staining time, and temperature. Cook et al. (96) have recently reported that 50 μM MCB are sufficient to label most of the GSH in rodent cells; however, it appears that the Km toward MCB for human GSTs is much higher, suggesting that an appropriate concentration may be closer to 1 mM MCB. Moreover, there are different isozymes of GST in different cell types; classes described include α, μ, and π forms, grouped according to their mobility on isoelectric focusing gels. The GST isozymes are homo- and heterodimes of peptides coded from multiple genes (105). Heterogeneity in the expression of the different isozymes of GST in different cell types, coupled with the fact that different GST isozyme classes show different reactivity toward MCB (GST-μ > GST-α > GST-π) (96, 101), means that one must be very careful to substantiate flow cytometric data with other conventional biochemically based assays of GSH (see below). This caveat is especially relevant when examining human tumor cells, many of which express primarily GST-π, the isoform with the lowest reactivity toward MCB. Caution is also appropriate in the use of MCB for measurement of GSH in human lymphocytes, since there is differential expression of a GST-π form (GST-λ), depending upon culture conditions and growth state (106), and since GST-μ expression has been shown to be polymorphic in PBL from humans, as indicated by reactivity toward trans-stilbene oxide (TSO) and benzo-a-pyrene-4,5-oxide (BPO) (106–110). In fact, if GST-μ shows the same polymorphic distribution in the human population toward MCB as it does towards TSO and BPO, then MCB/FCM would be a convenient assay for the polymorphic expression of this isozyme, the expression of which has been associated with a decreased risk for certain cancers (108–111).

Figure 31.13*A* shows a comparison of human T-cells stained with MCB at two different concentrations. It is obvious that the fluorescence of these cells is much higher when one stains with 1 mM MCB. We have also found, in contrast to Cook et al. (96), that the rate of GSH conjugation in human cells is temperature–dependent. As seen in Figure 31.13*A*, a significantly faster rate of fluorescence development is achieved when cells are incubated at 37°C rather than at room temperature, and the relative difference is greater with 60 μM MCB than with 1000 μM MCB. This result is consistent with the observations of Seidegärd and colleagues (108) who showed that the maximum activity toward TSO occurs at 40°C in peripheral blood mononuclear cells. In the studies published by Cook et al. (96) and Ublacker et al. (101), cells were reacted with MCB at room temperature (although it is mentioned in a footnote to the Cook paper that they did not see a temperature dependence in the cell types they examined). Both of these groups have addressed the limitations of the MCB/FCM method when measuring GSH in human cells (especially tumor cells). The specificity of the various GST isozymes toward MCB as a function of temperature needs to be more fully explored.

Figure 31.13*B* shows that rodent cells (Rat-1 fibroblasts) exhibit more rapid and higher MCB staining with lower concentrations than human lymphocytes, which is consistent with Cook et al. (96). Note, however, that appreciable differences between 60 μM and 1000 μM MCB still remain, and that the temperature used for incubation has a smaller, but still reproducible, effect than is seen with human T-cells. Thus, for both rodent cells (Rat-1 fibroblasts) and human cells (PBL), the concentration of dye used can substantially affect the amount of fluorescence seen on the cell sorter. The choice of a dye concentration depends upon the cell type being used, the Km for MCB for the GST isozymes of those cells, and the proportion of GSH one wishes to derivatize within the cell. Even with these higher concentrations of MCB, not all of the GSH has been derivatized. The basis for this incomplete derivatization has been attributed to the inhibition of GST by the GSH-bimane conjugate (96).

Nonetheless, we have found that lower concentrations of MCB (60 μM) may be used with human lymphocytes to reflect qualitative differences in GSH level. If one wishes only to determine if there is a correspondence of some parameter with relative GSH content, and not the exact amount of GSH present, these lower concentrations of MCB may suffice (see calibration section below).

PRACTICAL CONSIDERATIONS FOR STAINING WITH MCB

Stock solutions of the dye are prepared either in ethanol or DMSO, such that at the final working concentration the total

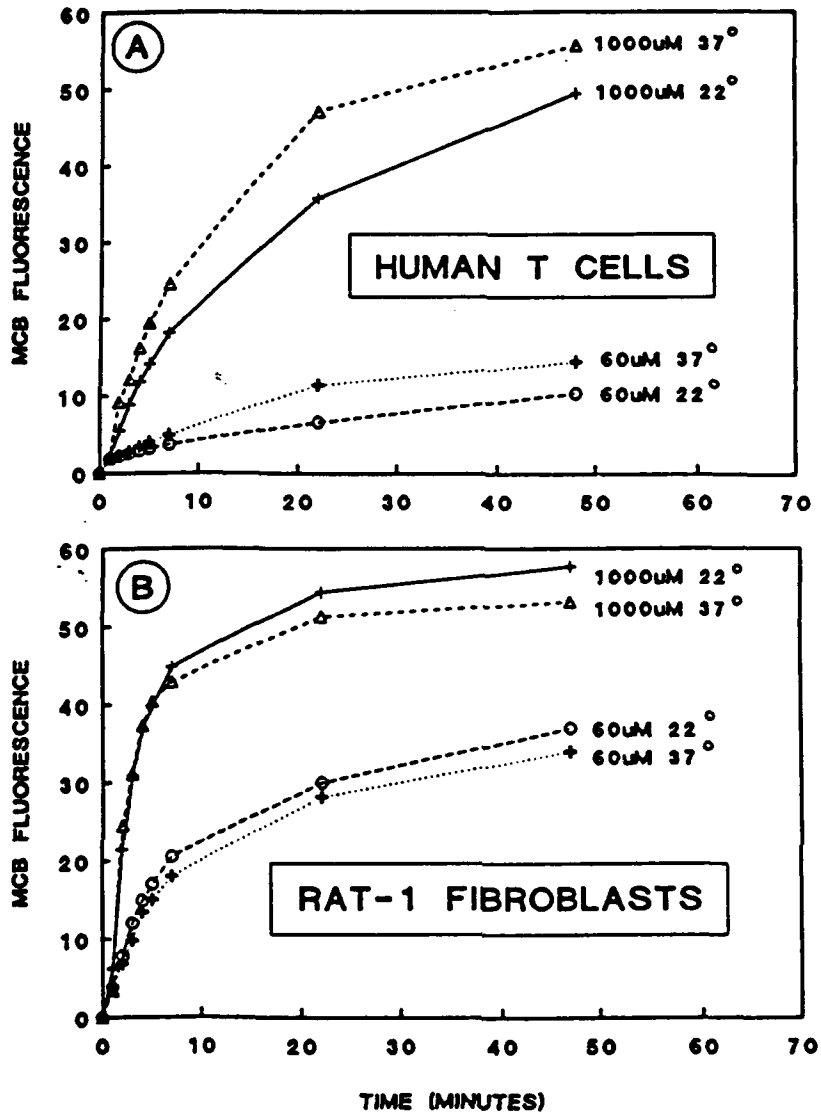

Figure 31.13. Influence of temperature and concentration on the kinetics of fluorescence development in MCB-stained *human T-cells* and *rat-1 fibroblasts*. *Human T-cells* from normal donors were isolated after density-gradient centrifugation. Cells were then left at room temperature or prewarmed in a 37°C water bath and placed in a fluorescence-activated cell sorter (Epics Elite, Coulter Corp., Hialeah, FL) with excitation at 328 nm and emission detected at 410–480 nm. After determining the baseline autofluorescence, the cells were quickly removed from the machine and an aliquot of these cells was transfered to another tube containing MCB that had been held at the appropriate temperature. This tube was quickly placed back into the machine and fluorescence development monitored over time. A shows MCB-stained *human T-cells*, B shows *rat-1 fibroblasts*. Both cell types developed fluorescence at a faster rate when stained with MCB at 1000 μM than when stained at 60 μM. *Human T-cells* showed a greater temperature dependence for this reaction than did *rat-1 fibroblasts*.

volume of the ethanol or DMSO does not exceed 1% of the cell suspension. These reagents can be stored at 4°C in the dark for up to one month. Cells are incubated with the desired concentration of MCB in medium, for the length of time desired, at 22°C or 37°C. After staining, cells are kept on ice and protected from light until analysis is performed on the flow cytometer.

MCB is nonfluorescent, but when conjugated to GSH by GST it is converted to the fluorescent GSH-bimane product. This reaction occurs in most cells, but since it does require GST, rates of formation of fluorescent product are variable depending upon the activities and specificities of the various isoenzymes of GST among cell types. However, there may also be pools of GSH unavailable for conjugation by this reagent in intact cells, such as within mitochondria.

CMFDA

As with MCB, CMFDA concentrations are expected to be cell-type-specific. We have previously reported experiments with Rat-1 fibroblasts using this reagent. Cells are stained in the dark with a 50 μM solution (final) for 10 min (or longer if nonspecific esterase activity is low) at 37°C. Stock solu-

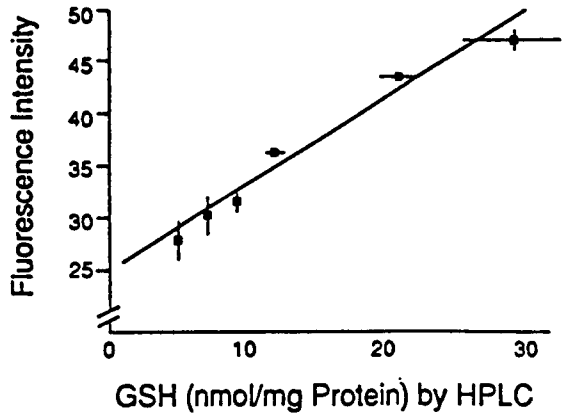

Figure 31.14. Correlation between GSH content measured by HPLC and MCB/flow cytometry. Chinese hamster V79 cells were treated with 0, 1, 3, 6, 9, or 12 mM BSO for 12 hr. Cells were then processed for flow cytometry (45 mM MCB for 10 min at 37°C) or for HPLC determination of total reduced GSH content. (Reprinted with permission from Kavanagh TJ, Martin GM, Livesey TC, Rabinovitch PS. Direct evidence of intercellular sharing of glutathione via metabolic cooperation. J Cell Physiol 1988;137:353–359.)

tions are made up with 5 mM in DMSO. If the cells are to be stained in medium, care should be taken to minimize or exclude serum in the medium, since serum contains variable esterase activity that will convert the reagent extracellularly to a cell impermeant form.

Calibration and Data Analysis

CALIBRATION BY HIGH-PERFORMANCE LIQUID CHROMATOGRAPHY (HPLC) AND TIETZE ASSAY

Since MCB fluorescence is dependent upon GST activity, and since CMFDA stains thiols and is not necessarily specific for GSH (although under most circumstances GSH is the major low-molecular-weight-thiol in cells), it is important to calibrate the level of fluorescence measured by flow cytometry with a more specific biochemical measure of GSH. We have used HPLC analysis and various doses of the GSH-depleting agent buthionine sulfoximine (BSO; an inhibitor of γ-glutamylcysteine synthetase) to ascertain the correlation between MCB fluorescence and GSH content in matched samples of Chinese hamster V79 cells (112). For this cell type, there is a very good correlation between mean cellular fluorescence by flow cytometry and GSH content by HPLC (Fig. 31.14).

In order to determine MCB specificity for GSH, one can simply run stained cell lysates over an HPLC column with fluorescence detection and compare with known low-molecular-weight-thiol standards that have been derivatized with MBB (70). When this is done, we find that >99% of the MCB fluorescence is associated with the GSH peak in protein-free cytosolic extracts of normal human PBL.

Another method of calibration is the Tietze recycling assay (113) or a modified version designed to handle multiple samples in a microtiter plate (114).

Since many flow cytometric applications of the use of MCB will be concerned with relative differences in GSH content among different cell populations, a highly relevant calibration procedure is to examine cells with different GSH content by both FCM and HPLC or biochemical assay. MCB is easily used to discriminate between the degrees of GSH depletion after treatments that oxidize or deplete intracellular GSH. Figures 31.15*A* and 31.15*B* show a series of histograms of human $CD4^+$ and $CD8^+$ lymphocytes pretreated with various doses of 1-chloro-2,4-dinitrobenzene (CDNB; a GSH depleter). A dose-dependent reduction in MCB fluorescence (after correction by subtraction of autofluorescence) is seen with increasing concentrations of CDNB in both T-cell subsets. The measurement of the relative decline of MCB fluorescence as a function of CDNB concentration used for MCB depletion reveals that the lower concentration of MCB (60 μM) shows a greater relative depletion with increasing doses of CDNB than does staining with 1 mM MCB (Fig. 31.15*C*), and a closer correspondence with GSH concentration, as determined by HPLC (Fig. 31.15*E*). This suggests that a greater proportion of the MCB staining at 1 mM is attributable to nonspecific staining of protein thiols and that, in spite of the lower proportion of total GSH stained with 60 μM MCB (Fig. 31.13*A*), this staining concentration may yield a more linear relationship to alterations in GSH content in this cell type. Figures 31.15*D* and 31.15*F* show 25% to 40% CDNB-resistant staining with MBB (higher with higher MBB concentration), a result that is consistent with the staining of other non-GSH thiols by MBB. For each staining protocol used in Figure 31.15, there was little difference between $CD4^+$ PBL, $CD8^+$ PBL, and $CD4^-CD8^-$ PBL (primarily B-cells). Data, such as that in Figure 31.15, suggest that, while absolute and intercell-type comparisons of GSH using MCB may be more difficult, measurement of relative differences may be much more reliable in human lymphocytes. This result is in agreement with the study of rodent cells by Ublacker et al. (101), but is in contrast with the results they obtained with human tumor and monkey cells. The latter showed disparity between flow cytometric GSH quantitation and biochemical assay. As described previously, this may be related to the predominance of the GSH-π isoform in these tumor cells, which has the highest Km for MCB. Thus, while MCB fluorescence can, in some cell types, yield excellent correlation with GSH, this may not be the case in other cell types, and reliance upon the flow cytometric determinations should be made only after careful study of the relationship of MCB fluorescence to independent assays of GSH content.

GST ACTIVITY

As discussed above, heterogeneity among cell types exists with respect to the total GST activity, the isozymes expressed, and their Km toward MCB. It is therefore important to address the question of GST activity toward MCB in a particular cell type in order to insure that one is using the

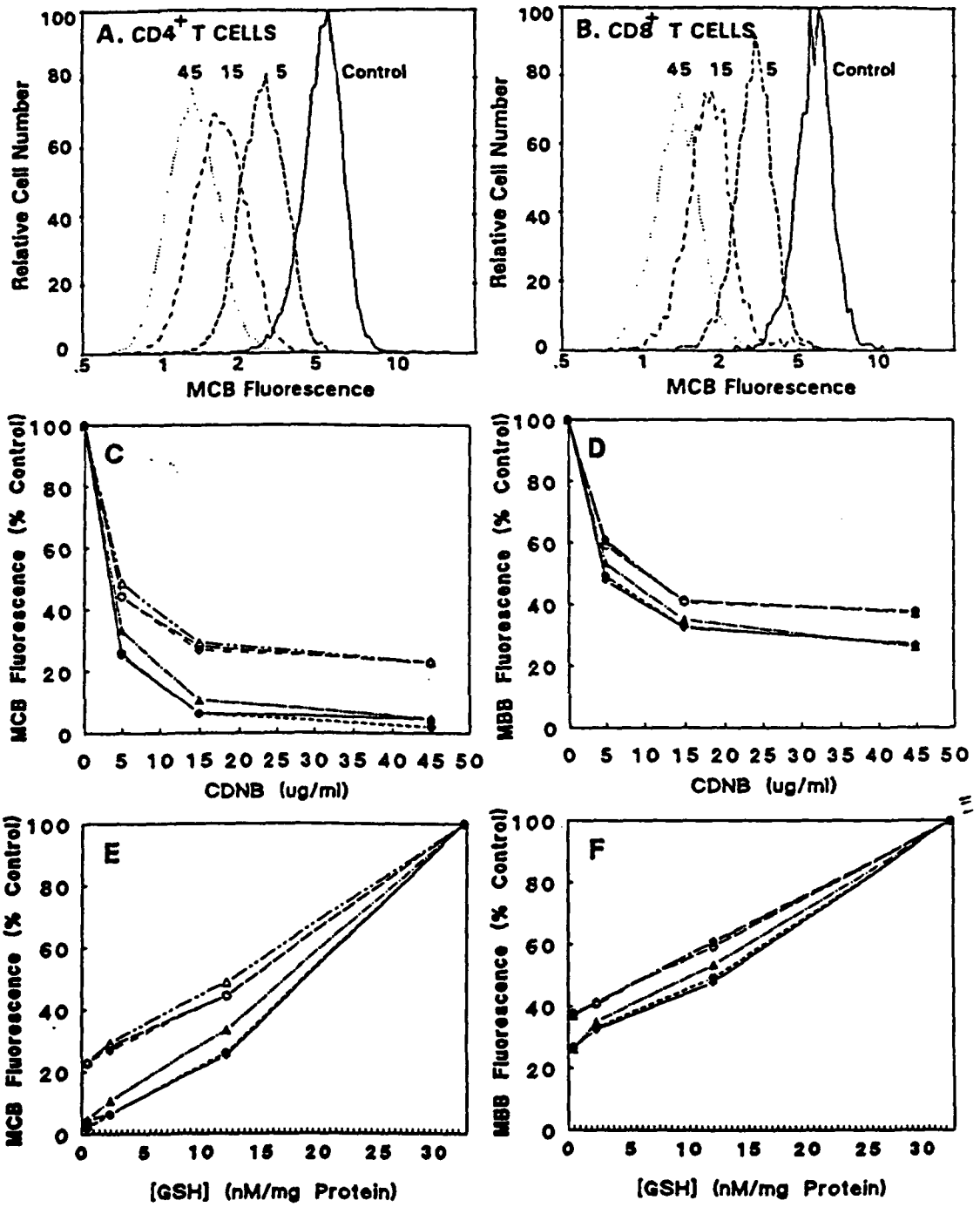

Figure 31.15. Effect of treatment with 1-chloro-2,4-dinitrobenzene (CDNB) on the GSH content of human CD4+ and CD8+ PBL as determined with MCB/flow cytometry and HPLC. A and B show MCB (60 μM) fluorescence histograms of CD4+ and CD8+ cells pretreated with CDNB at 0, 5, 15, and 45 mg/ml for 15 min at 37°C. C shows the effect of using two different concentrations of MCB (60μM, closed symbols, and 1 mM, open symbols) on the measurement of CDNB-induced decline in fluorescence as a percentage of the fluorescence of the nontreated controls. D shows a similar analysis for MBB (60 μM and 1 mM). There is a similar proportionate decline in fluorescence for CD4+ cells (*diamonds*), CD8+ cells (*circles*) and CD4-,CD8- cells (*triangles*), regardless of which concentration of MCB or MBB was used. E compares the level of GSH-bimane conjugate (as determined by HPLC in PBL stained with 1 mM MBB) with the mean relative fluorescence of CD4+ cells, CD8+ cells, and CD4-,CD8- cells stained with either 60 μM or 1 mM MCB. F shows a similar comparison for 60 μM ro 1mM MBB. Autofluorescence of unstained cells has been subtracted from all fluorescence intensities plotted in panels *C–F*.

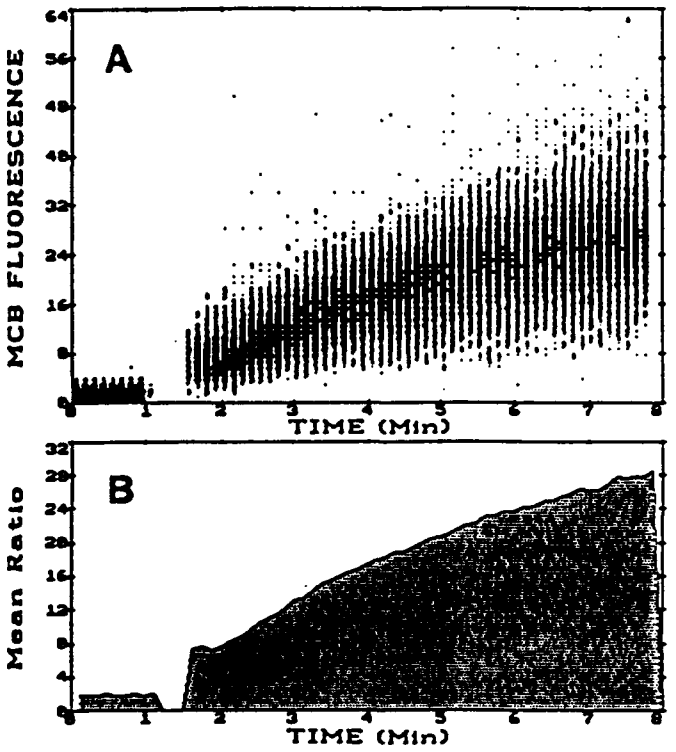

Figure 31.16. MCB fluorescence cytogram (A) showing the kinetics of MCB conjugation in human CD4⁺ lymphocytes by flow cytometry. CD4⁺ cells isolated on density gradients from peripheral blood were resuspended in RPMI medium at a concentration of 10^6 cells/ml, and warmed to 37°C. After establishing a baseline (auto)fluorescence for 1 min, a 0.5-ml aliquot of the cells was then transferred to a prewarmed (37°C) tube containing MCB, such that the final concentration was 1 mM. This tube was quickly placed back in the cell sorter and the analysis was continued for a total of 8 min. One not only can determine the mean GST activity from such data, but also an indication of intercellular heterogeneity in the GST activity. The mean MCB fluorescence vs. time is shown in B.

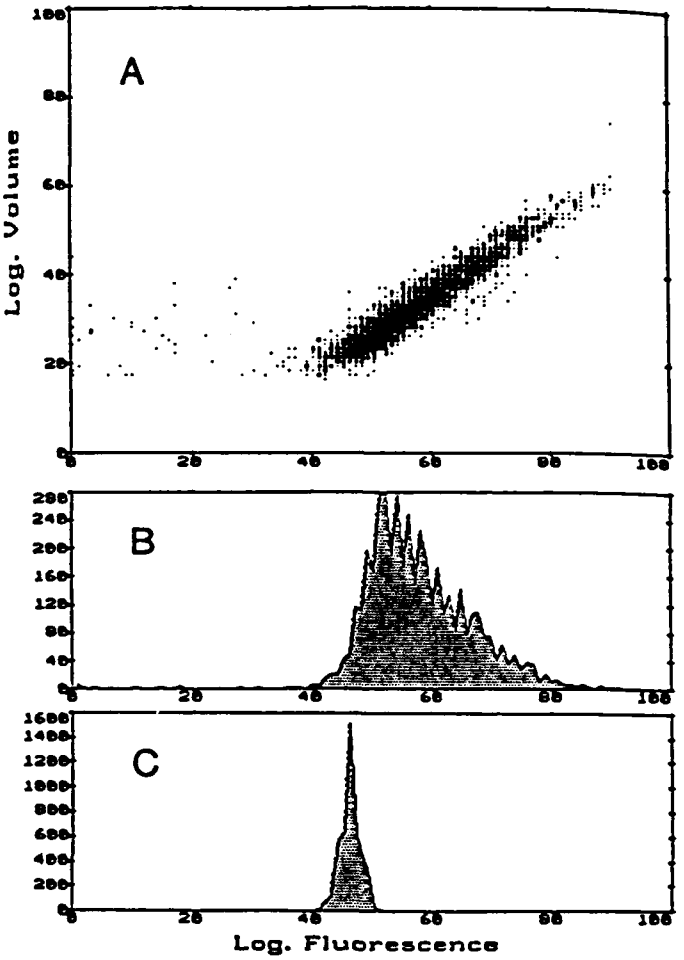

Figure 31.17. Relationship between cell size and GSH content as determined by MCB/flow cytometry. A shows a bivariate cytogram (log electronic volume vs. log fluorescence) of rat-1 fibroblasts stained with MCB. There is a direct relationship between cell size and fluorescence intensity, indicating that the concentration of GSH in these cells is tightly controlled, independent of cell size. B and C show histograms of fluorescence data not corrected for volume and corrected for volume, respectively. The logarithmic axes correspond to a three-decade range.

appropriate MCB staining concentration, incubation time, and temperature. Watson et al. (115) and Cook et al. (96) have described the use of MCB to assess GST activity in cells. An example of this type of analysis is presented in Figure 31.16. Cells in suspension are held at room temperature or prewarmed to 37°C, and a baseline autofluorescence is established for 30 sec to 1 min. Analysis is briefly interrupted and a predetermined aliquot of these cells is added to a room temperature or prewarmed tube containing MCB. The suspension is then quickly analyzed for accumulation of fluorescence over time (usually 10 min) at the preferred temperature. Initial rates of fluorescence accumulation are indicative of GST activity.

DATA ANALYSIS

Since GSH concentration but not absolute content, is regulated in the cell, it is important to compensate for heterogeneity in cell volume when assessing cellular GSH by flow cytometry. We have found that simultaneous measurement of GSH-dependent fluorescence and electronic cell volume yields data that can easily be adjusted for cell volume bias in GSH content (Fig. 31.17*A*). By acquiring data on log scale for both volume and MCB fluorescence, one can more easily distinguish between control and GSH-depleted cell populations. Compensation for volume by analyzing the ratio of log fluorescence to log volume, allows one to appreciate diffrences that would otherwise be complicated by volume effects (112) (Figures 31.17*B* and 31.17*C*). MCB analysis on instruments that rely on sizing of the cells with forward-angle light scatter can be made either by gating on a specific cell size to minimize volume effects, or by displaying bivariate histograms of the ratio of log fluorescence to log forward scatter.

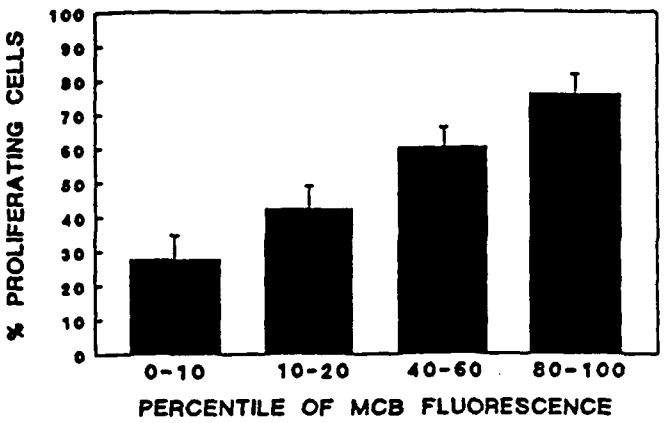

Figure 31.18. Proliferation of human CD4⁺ lymphocytes sorted on MCB fluorescence intensity. Human lymphocytes isolated from peripheral blood by density gradient centrifugation were stained with MCB (60 μM for 15 min at 37°C) and PE anti-CD4 mAb. CD4⁺ cells were then sorted according to their MCB fluorescence for the lowest 10%, 10th to 20th percentile, 40th to 60th percentile, and the highest 20% of the fluorescence histogram. Cells were then plated into 96-well plates precoated with anti-CD3 mAb in BrdU-containing medium. After three days, cells were harvested and assessed for proliferation by the BrdU/Hoechst method (129). There is a direct correlation between the MCB fluorescence intensity of the unstimulated cells and their subsequent ability to proliferate. (Data kindly provided by Dr. A. Grossman.)

Role of GSH in Cell Activation

A large number of studies have shown that GSH is important for cell activation and replication. Most of these studies relied on the disruption of normal GSH homeostasis with drugs that either deplete or enhance GSH content in order to show a GSH dependence for cell growth or function (69, 116–124).

An alternative approach to the study of lymphocyte activation is to sort on the basis of GSH content and then to assess growth in the sorted cells after they are allowed to recover to their pretreatment levels of GSH (70). There is a direct correlation between initial GSH content in unstimulated CD4⁺ human lymphocytes and the capacity for subsequent cell proliferation (Fig. 31.18). In an attempt to ascertain the GSH-sensitive steps in cell proliferation, we stained cells sorted on their GSH content with acridine orange in order to assess their RNA and DNA content simultaneously; this allows one to distinguish activated G_1 cells from those that remain quiescent (G_0) (122). Figure 31.19 shows that cells with low GSH remain in G_0 after mitogen stimulation, suggesting that there is an early step in cell activation that is blocked in low GSH cells.

The effect of GSH content on very early steps in transmembrane signal transduction can be directly evaluated by using indo-1 to assess mitogen-induced changes in intracellular calcium. Figure 31.20 shows the effects of pretreating CD4⁺ cells with *n*-ethylmaleimide (NEM) on their ability to respond to stimulation with anti-CD3 mAb. As is apparent

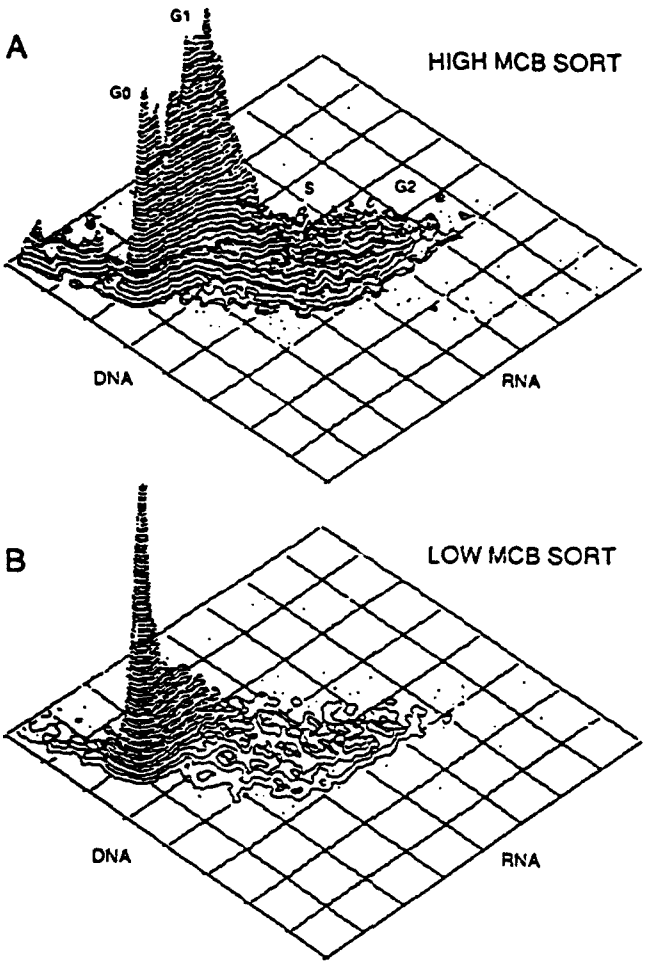

Figure 31.19. Effect of GSH status on the ability of CD4⁺ cells to become activated by anti-CD3 mAb, as determined by RNA synthesis. Cells were stained with 60 μM MCB and sorted on GSH content (upper and lower 30% of fluorescence histogram distribution), allowed to recover for 24 hr, and stimulated with solid phase anti-CD3 mAb. After 48 hr, cells were fixed in ethanol, stained with acridine orange, and analyzed by flow cytometry for RNA and DNA content. Cells with high GSH (*high MCB sort*) show the ability to exit G_0 (A), as demonstrated by elevated RNA content in G_1, *S*, and G_2 cells, whereas cells sorted for low GSH content have nearly all remained in G_0 (B). (Reprinted with permission from Kavanagh TJ, Grossman A, Jaecks EP, et al. Proliferative capacity of human peripheral blood lymphocytes sorted on the basis of glutathione content. J Cell Physiol 1990;145: 472–480.)

from the figure, this reagent, which effectively depletes GSH (Fig. 31.20*B*), as well as some protein thiols (126), dramatically reduced calcium signaling in CD4⁺ cells. In contrast to the results with T-cells, B-cells pretreated with NEM do not show similar reductions in calcium signaling (data not shown), indicating that these two classes of lymphocytes have very different thiol-redox requirements for their activation. To directly assess the relationship of GSH to transmembrance signaling, we have sorted CD4⁺ cells on the basis of their GSH content and subsequently evaluated mitogen-induced changes in indo-1 ratio. As shown in Figure 31.21, cells with high GSH show more vigorous $[Ca^{2+}]_i$

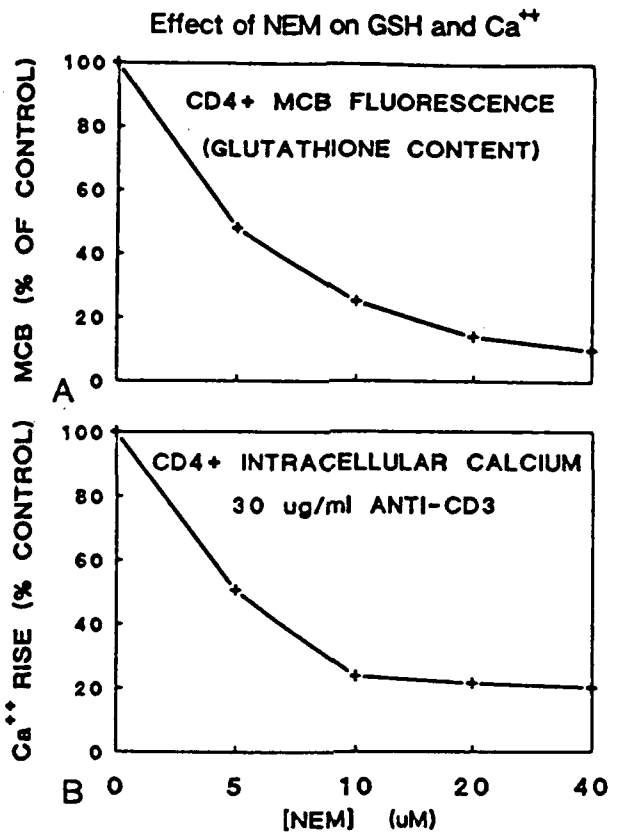

Figure 31.20. Effect of depletion of intracellular thiols upon intracellular calcium signaling. Indo-1-loaded cells were exposed to various concentrations of NEM, which progressively deplete GSH (A). The cells were stimulated with 30 μg/ml anti-CD3 mAb and $[Ca^{2+}]_i$ was examined. There is a progressive inhibition of the rise in $[Ca^{2+}]_i$ as a function of increasing NEM concentration (B).

responses than cells with low GSH. These results suggest the possibility that certain components of the transmembrane signaling apparatus in at least some cell types are sensitive to thiol oxidation. It is known, for instance, that p56*lck* contains a zinc finger motif and this should be sensitive to oxidation. Freed et al. (126) have assessed the influence of membrane thiol groups in lymphocyte proliferation, IL-2 production, and receptor expression, and have reported similar findings. Surface thiol groups are also important for the activation of neutrophils and monocytes (127).

GSH Variations During the Cell Cycle: Simultaneous Evaluation of DNA and GSH

The ability of CMFDA to be used as a thiol stain excited with visible light has made it possible to simultaneously evaluate GSH levels and DNA content in viable proliferating populations of cells (104). Figure 31.22 shows a bivariate cytogram of Rat-1 fibroblasts stained for GSH with CMFDA and DNA with Hoechst 33342. As one can appreciate from the figure, there is a twofold increase in fluorescence in G_2 cells; this increase appears consistent with their increase in cell volume. The ability to evaluate GSH and DNA simultaneously will surely facilitate the identification of drug-resistant tumor cells from biopsy material, allowing one to ascertain relationships between aneuploidy and changes in GSH content and/or GST activity.

Sorting on the Basis of GSH: Isolation of GSH Variants

Since MCB is a viable stain, one can sort cells on the basis of their GSH content. Lee and Siemann (128) have used MCB and cell sorting to isolate human ovarian tumor cells with increased GSH content that were also resistant to adriamycin. However, the cells reverted to normal GSH after growth in culture over time. Using repeated rounds of MCB staining and sorting, a number of Rat-1 fibroblast variants that have stable alterations in their basal GSH content have been isolated (Fig. 31.23). These cells have not yet been characterized as to the basis of their altered GSH level. However, likely possibilities include mutations in the genes coding one of the two enzymes responsible for GSH synthesis (γ-glutamylcysteine synthetase; glutathione synthetase), differential expression of GST isozymes, or deficiencies in cysteine transport. High GSH variants may have mutations

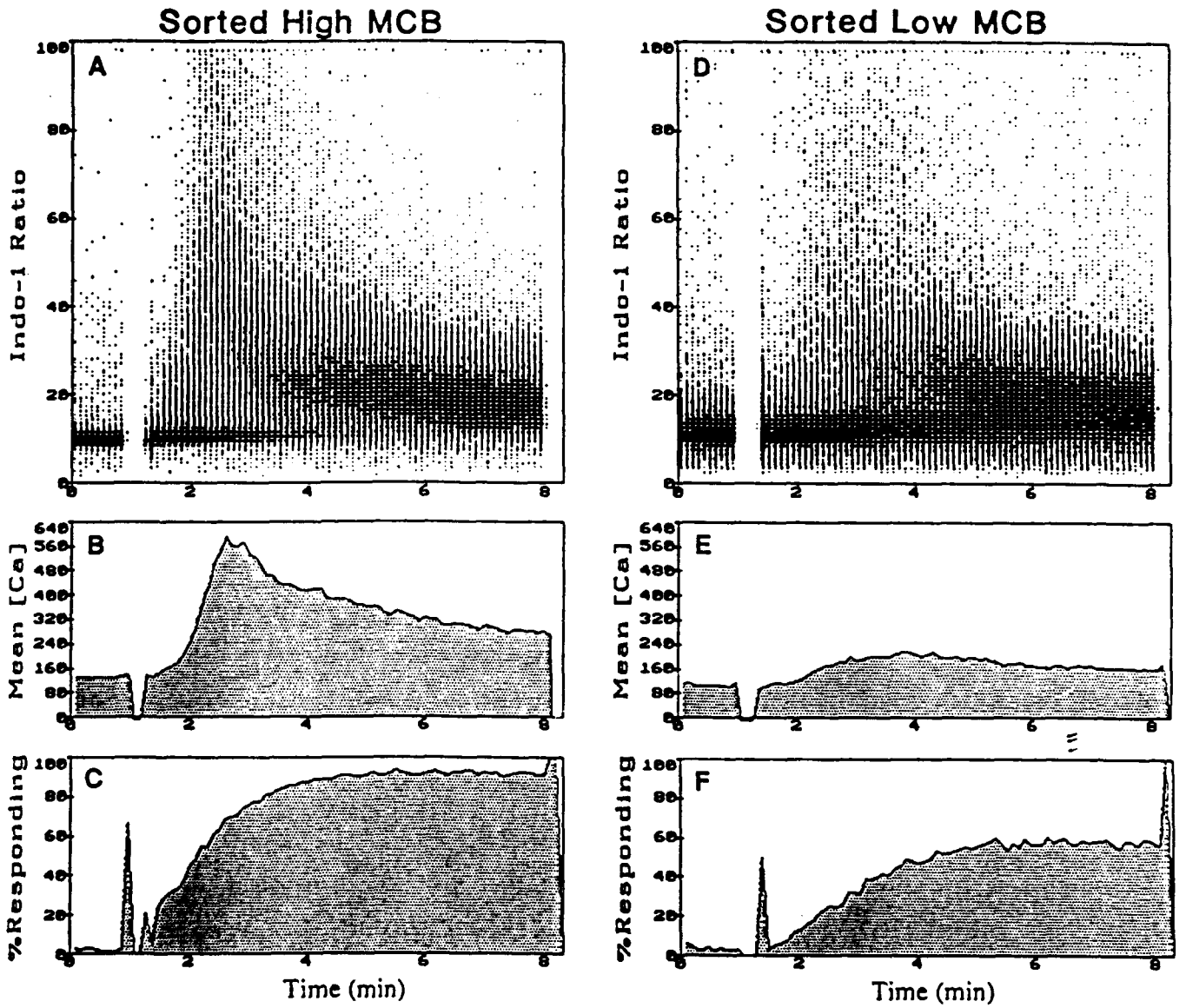

Figure 31.21. Effect of intracellular GSH content on anti-CD3 mAb-stimulated transmembrane signal transduction in CD4⁺ human T-lymphocytes. Human PBL were stained with 60 mM MCB and PE-anti-CD4 mAb. CD4⁺ cells were sorted as the upper and lower 30% of the MCB fluorescence distribution, allowed to recover for 24 hr, and then loaded with either indo-1 AM or restained with MCB. Cells restained with MCB retained their originally sorted MCB fluorescence differences (not shown). Cells loaded with indo-1 were analyzed for $[Ca^{2+}]_i$ content following stimulus with anti-CD3 mAb (as described in Fig. 31.4). A and D show the kinetics of $[Ca^{2+}]_i$ transients in cells sorted on high and low GSH content, respectively. There is a diminished response in cells with low GSH content. B and E show the mean $[Ca^{2+}]_i$ calculated from the data presented in A and D, respectively. There is a higher mean and peak calcium response in the high GSH-sorted cells than in the low GSH-sorted cells. C and F show the percentage of responding cells calculated from the data presented in A and D, respectively. There is an appreciably higher percentage of cells that are able to respond in the high GSH-sorted cells than in the low GSH-sorted cells.

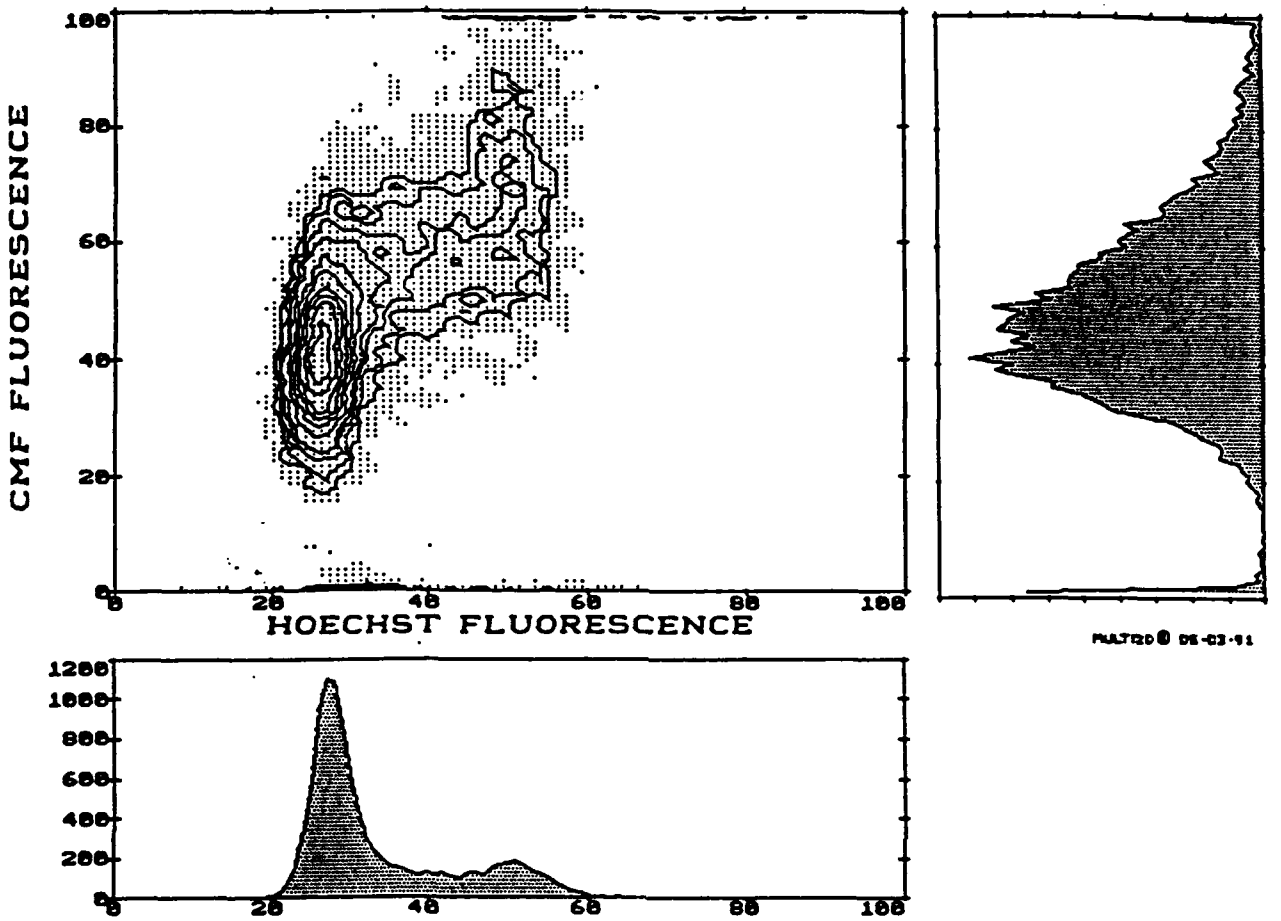

Figure 31.22. Simultaneous measurement of DNA and thiol content in rat-1 fibroblasts. Live cells were stained with Hoechst 33342 (10 mM) for 30 min at 37°C. During the last 10 min of Hoechst staining, the cells were stained with CMFDA (10 mg/ml). Cells were then analyzed with a dual-laser cell sorter. DNA-specific fluorescence was measured with UV excitation and blue emission. The temporarily delayed signal from CMF fluorescence was measured with 488-nm excitation and green emission. Cell aggregates were gated from the analysis by displaying Hoechst-42 fluorescence vs. peak area (not shown).

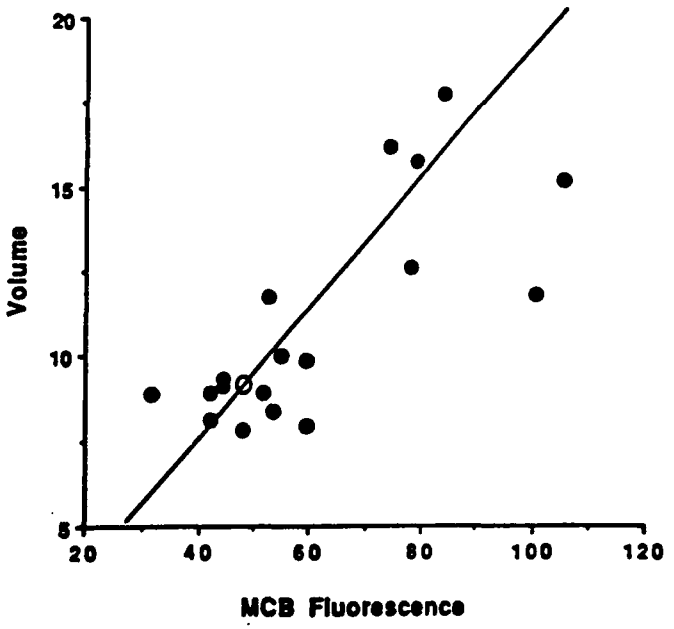

Figure 31.23. MCB fluorescence and electronic cell volume of rat-1 fibroblast GSH variants isolated after several rounds of MCB staining and viable sorting. Rat-1 fibroblasts were stained with MCB (45 μM for 10 min at 37°C), placed in a cell sorter, and sorted on the highest and lowest 5% of the fluorescence histogram. Cells were then allowed to recover and grow to confluence, at which time the process was repeated until separate populations of cells appeared. The cells were then individually sorted into wells of a 96-well tissue culture plate and grown from single cell clones. The figure represents mean volume and fluorescence of these variants after analysis on a FACS Analyzer. The nonselected parental cells are shown as an open symbol. Note that clones lying above the line from the origin through the parental cells have lower intracellular MCB *concentrations* than the parental cells (although many such cells had larger volumes), while clones below this line have an increased intracellular MCB concentration.

in the regulation of these genes resulting in increased amounts of product, such that there is an abnormally high level of GSH synthesis or conjugation.

ACKNOWLEDGMENTS

We thank J.A. Ledbetter and A. Grossmann for many valuable comments, D.L. Eaton for providing HPLC analysis, and J.C. Jinneman and R.C. Lee for their much-valued technical assistance. This work ws supported in part by the Naval Medical Research and Development Command, Research Task No. M0095.003-1007, and by the National Institutes of Health Grant AG01751. The opinions and assertions expressed herein are those of the authors and are not to be construed as official or reflecting the views of the Navy Department or the naval service at large.

REFERENCES

1. Blinks JR, Wier WG, Hess P, Prendergast FG. Measurement of Ca^{++} concentrations in living cells. Prog Biophys Mol Biol 1982;40:1–114.
2. Tsien RY, Pozzan T, Rink TJ. Calcium homeostasis in intact lymphocytes: cytoplasmic free calcium monitored with a new, intracellularly trapped fluorescent indicator. J Cell Biol 1982;94:325–334.
3. Tsien RY. A non-disruptive technique for loading calcium buffers and indicators into cells. Nature 1981;290:527–528.
4. Ransom JT, DiGiusto DL, Cambier JC. Single cell analysis of calcium mobilization in anti-immunoglobulin-stimulated B lymphocytes. J Immunol 1986;136:54–57.
5. Grynkiewicz G, Poenie M, Tsien RY. A new generation of Ca2+ indicators with greatly improved fluorescence properties. J Biol Chem 1985;260:3440–3450.
6. Minta A, Kao JPY, Tsien RY. Fluorescent indicators for cytosolic calcium based on rhodamine and fluorescein chromophores. J Biol Chem 1989;264:8171–8178.
7. Tsien RY. Fluorescent indicators of ion concentrations. Methods Cell Biol 1989;30:127–156.
8. Vandenberghe PA, Ceuppens JL. Flow cytometric measurement of cytoplasmic free calcium in human peripheral blood T-lymphocytes with fluo-3, a new fluorescent calcium indicator. J Immunol Methods 1990;127:197–205.
9. Rijkers GT, Justement LB, Griffioen AW, Cambier JC. Improved method for measuring intracellular Ca^{++} with fluo-3. Cytometry 1990;11:923–927.
10. Rabinovitch PS, June CH, Grossmann A, Ledbetter JA. Heterogeneity among T cells in intracellular free calcium responses after mitogen stimulation with PHA or anti-CD3. Simultaneous use of indo-1 and immunofluorescence with flow cytometry. J Immunol 1986;137:952–961.
11. Cohen LB, Salzberg BM, Davila HV, et al. Changes in axon fluorescence during activity: Molecular probes of membrane potential. J Membr Biol 1974;19:1–36.
12. Poenie M, Alderton J, Steinhardt R, Tsien R. Calcium rises abruptly and briefly throughout the cell at the onset of anaphase. Science 1986; 233:886–889.
13. Chused TM, Wilson HA, Greenblatt D, et al. Flow cytometric analysis of murine splenic B lymphocyte cytosolic free calcium response to anti-IgM and anti-IgD. Cytometry 1987;8:396–404.
14. Davies TA, Drons D, Weil GJ, Simons ER. Flow cytometric measurements of cytoplasmic calcium change in human platelets. Cytometry 1988;9:138–142.
15. Miller RA, Jacobson B, Weil G, Simons ER. Diminished calcium influx in lectin-stimulated T cells from old mice. J Cell Physiol 1987; 132:337–42.
16. Parks DR, Nozaki T, Dunne JF, Peterson LL. Flow cytometer adaptation for quantitation of immunofluorescent reagents and for calibration of dyes for measuring cellular Ca^{2+} and pH. Cytometry 1987;(Suppl 1):104.
17. Martell AE, Smith RM. Critical Stability Constants. Volume 1: Amino Acids. New York: Plenum Press, 1968;269–272.
18. Harafuji H, Ogawa, Y. Re-examination of the apparent binding constant of ethylene glycol bis(beta-aminoethyl ether)-N,N,N',N'-tetraacetic acid with calcium around neutral pH. J Biochem 1980;87: 1305–1312.
19. Moisescu DG, Pusch H. A pH-metric method for the determination of the relative concentration of calcium to EGTA. Pflugers Archiv 1975; 355:R122.
20. Miller DJ, Smith GL. EGTA purity and the buffering of calcium ions in physiological solutions. Am J Physiol 1984;246:C160–C166.
21. Overton, WR. Modified histogram subtraction technique for analysis of flow cytometric data. Cytometry 1988;9:619–626.
22. Rabinovitch PS, June CH. Intracellular ionized calcium, membrane potential, and pH. In: Olmerod MG, ed. Flow Cytometry: A Practical Approach. Oxford: Oxford Press, 1990;161–185.
23. Lazzari KG, Proto PJ, Simons ER. Simultaneous measurement of stimulus-induced changes in cytoplasmic Ca^{2+} and in membrane potential of human neutrophils. J Biol Chem 1986;261:9710–9713.
24. Ishida Y, Chused TM. Heterogeneity of lymphocyte calcium metabolism is caused by a T cell-specific calcium-sensitive potassium channel and sensitivity of the calcium ATPase pump to membrane potential. J Exp Med 1988;168:839–852.
25. Goldsmith MA, Weiss A. Isolation and characterization of a T-lymphocyte somatic mutant with altered signal transduction by the antigen receptor. Proc Natl Acad Sci USA 1987;84:6879–6883.
26. Goldsmith MA, Weiss A. Early signal transduction by the antigen receptor without commitment to T cell activation. Science 1988;240: 1029–1031.
27. De Virgilio F, Steinberg TH, Swanson JA, Silverstein SC. Fura-2 secretion and sequestration in macrophages. A blocker of organic anion transport reveals that these processes occur via a membrane transport system for organic anions. J Immunol 1988;140:915–920.
28. Malgawli A, Milani D, Meldolesi J, Pozzan T. Fura-2 measurement of cytosolic free Ca^{2+} in monolayers and suspensions of various types of animal cells. J Cell Biol 1987;105:2145–2155.
29. Steinberg SF, Bilezikian JP, Al-Awqati Q. Fura-2 fluorescence is localized to mitochondria in endothelial cells. Am J Physiol 1987;253(Pt 1):C744–C747.
30. Arslan P, DeVirgilio F, Beltrane M, Tsien RY, Dozzan T. Cytosolic Ca^{2+} homeostasis in Ehrlich and Yoshida carcinomas. J Biol Chem 1985;260:2719–2725.
31. Luckhoff A. Measuring cytosolic free calcium concentration in endothelial cells with indo-1: The pitfall of using the ratio of two fluorescence intensities recorded at different wavelengths. Cell Calcium 1986;7:233–248.
32. Scanlon M, Williams DA, Fay FS. A Ca2+-insensitive form of fura-2 associated with polymorphonuclear leukocytes. Assessment and accurate Ca2+ measurement. J Biol Chem 1987;262:6308–6312.
33. Anasetti C, Martin PJ, June CH, et al. Induction of calcium flux and enhancement of cytolytic activity in natural killer cells by cross-linking of the sheep erythrocyte binding protein (CD2) and the Fc-receptor (CD16). J Immunol 1987;139:1772–1779.
34. Geppert TD, Wacholtz MC, Davis LS, Lipsky PE. Activation of human T4 cells by cross-linking class I MHC molecules. J Immunol 1988;140:2155–2164.
35. June CH, Rabinovitch PS, Ledbetter JA. CD5 antibodies increase intracellular ionized calcium concentration in T cells. J Immunol 1987; 138:2782–2792.
36. Pezzutto A, Dörken B, Rabinovitch PS, Ledbetter JA, Moldenhauer G, Clark EA. CD19 monoclonal antibody HD37 inhibits anti-immunoglobulin-induced B cell activation and proliferation. J Immunol 1987;138:2793–2799.
37. Pezzutto A, Rabinovitch PS, Dorken B, Moldenhauer G, Clark EA. Role of the CD22 human B cell antigen in B cell triggering by anti-immunoglobulin. J Immunol 1988;188:1791–1795.

38. Wilson HA, Greenblatt D, Taylor CW, et al. The B lymphocyte calcium response to anti-Ig is diminished by membrane immunoglobulin cross-linkage to the Fc gamma receptor. J Immunol 1987;138:1712–1718.
39. Ledbetter JA, June CH, Grosmaire LS, Rabinovitch PS. Crosslinking of surface antigens causes mobilization of intracellular ionized calcium in T lymphocytes. Proc Natl Acad Sci USA 1987;84:1384–1388.
40. Ledbetter JA, June CH, Rabinovitch PS, Grossmann A, Tsu TT, Imboden JB. Signal transduction through CD4 receptors: stimulatory vs. inhibitory activity is regulated by CD4 proximity to the CD3/T cell receptor. Eur J Immunol 1988;18:525–532.
41. Poenie M, Tsien RY, Schmitt-Verhulst AM. Sequential activation and lethal hit measured by $[Ca^{2+}]_i$ in individual cytolytic T cells and targets. EMBO J 1987;6:2223–2232.
42. Williams DA, Becker PL, Fay FS. Regional changes in calcium underlying contraction of single smooth muscle cells. Science 1987;235: 1644–1648.
43. Ware JA, Smith M, Salzman EW. Synergism of platelet-aggregating agents. Role of elevation of cytoplasmic calcium. J Clin Invest 1987; 80:267–271.
44. Cobbold PH, Rink TJ. Fluorescence and bioluminescence measurement of cytoplasmic free calcium. Biochem J 1987;248:313–328.
45. Ambler SK, Poenie M, Tsien RY, Taylor P. Agonist-stimulated oscillations and cycling of intracellular free calcium in individual cultured muscle cells. J Biol Chem 1988;263:1952–1959.
46. Wilson HA, Greenblatt D, Poenie M, Finkelman FD, Tsien RY. Crosslinkage of B lymphocyte surface immunoglobulin by anti-Ig or antigen induces prolonged oscillation of intracellular ionized calcium. J Exp Med 1987;166:601–606.
47. June CH, Rabinovitch PS. Flow cytometric measurement of cellular ionized calcium concentration. Pathol Immunopathol Res 1988;7:409–432.
48. Rabinovitch PS, June CH. Measurement of intracellular free calcium and membrane potential. In: Melamed MR, Lindmo T, Mendelsohn ML, eds. Flow cytometry and cell sorting. Second Edition. New York: Wiley-Liss, 1990; 651–668.
49. Grossmann A, Rabinovitch PS. Flow cytometry with indo-1 reveals variation in intracellular free calcium within T-cell subsets and between donors after mitogen stimulation. In: Burger G, Ploem JS, Goerttler K, eds. Clinical cytometry and histometry. London: Academic Press, 1987;192–194.
50. Ledbetter JA, Rabinovitch PS, Hellström I, Hellström KE, Grosmaire LS, June CH. Role of CD2 crosslinking in cytoplasmic calcium responses and T cell activation. Eur J Immunol 1988;18:1601–1608.
51. Linette GP, Hartzman RJ, Ledbetter JA, June CH. HIV-1 infected T cells exhibit a selective transmembrane signalling defect through the CD3/antigen receptor pathway. Science 1988;241:573–576.
52. Thomas, RC. Bicarbonate and pHi response Nature 1989;337:601.
53. de Grooth BG, van Dam M, Swart NC, Willemsen A, Greve J. Multiple wavelength illumination in flow cytometry using a single arc lamp and a dispersing element. Cytometry 1987;8:445–452.
54. Valet G, Raffael A, Moroder L, Wünsch E, Ruhenstroth-Bauer G. Fast intracellular pH determination in single cells by flow-cytometry. Naturwissenschaften 1981;68:265–266.
55. Whitaker JE, Haugland RP, Prendergast FG. Seminaphtho-fluoresceins and -rhodafluors: dual fluorescence pH indicators. Biophys J 1988;53:197a.
56. Thomas JA, Buchsbaum RN, Zimniak A, Racker E. Intracellular pH measurements in Ehrlich ascites tumor cells utilizing spectroscopic probes generated in situ. Biochemistry 1979;18:2210–2218.
57. Meister A. Glutathione metabolism and its selective modification. J Biol Chem 1988;263:17205–17208.
58. Meister A, Anderson ME. Glutathione. Ann Rev Biochem 1983;52: 711–760.
59. Reed DJ. Glutathione: Toxicological implications. Annu Rev Pharmacol Toxicol 1990;30:603–631.
60. Brodie AE, Reed DJ. Cellular recovery of glyceraldehyde-3-phosphate dehydrogenase activity and thiol status after exposure to hydroperoxides. Arch Biochem Biophys 1990;276:212–218.
61. Joshi TG, Schirch V. The role of a critical sulfhydryl group in the mechanism of serine hydroxymethyltransferase. Ann NY Acad Sci 1990;585:339–345.
62. Nalecz KA, Müller M, Zambrowicz EB, Wojtczak L, Azzi A. Significance and redox state of SH groups in pyruvate carrier isolated from bovine heart mitochondria. Biochim Biophys Acta 1990;1016:272–279.
63. Niroomand F, Rössle R, Mülsch A, Böhme E. Under anaerobic conditions, soluble guanylate cyclase is specifically stimulated by glutathione. Biochem Biophys Res Commun 1989;161:75–80.
64. Sun Y, Oberley LW. The inhibition of catalase by glutathione. Free Radic Biol Med 1989;7:595–602.
65. Suzuki M, Capparelli AW, Jo OD, Yanagawa N. Thiol redox and phosphate transport in renal brush-border membrane. Biochim Biophys Acta 1990;1021:85–90.
66. Zeigler DM. Role of reversible oxidation-reduction of enzyme thiols-disulfides in metabolic regulation. Ann Rev Biochem 1985;54:305–329.
67. Leung MF, Chou IN. Relationship between 1-chloro-2,4-dinitrobenzene-induced cytoskeletal perturbations and cellular glutathione. Cell Biol Toxicol 1989;5:51–66.
68. Messina JP, Lawrence DA. Cell cycle progression of glutathione-depleted human peripheral blood mononuclear cells is inhibited at S phase. J Immunol 1989;143:1974–1981.
69. Suthanthiran M, Anderson ME, Sharma VK, Meister A. Glutathione regulates activation-dependent DNA synthesis in highly purified normal human T lymphocytes stimulated via the CD2 and CD3 antigens. Proc Natl Acad Sci USA 1990;87:3343–3347.
70. Kavanagh TJ, Grossmann A, Jaecks EP, et al. Proliferative capacity of human peripheral blood lymphocytes sorted on the basis of glutathione content. J Cell Physiol 1990;145:472–480.
71. Meister A. 5-Oxoprolinuria (pyroglutamic aciduria) and other disorders of the γ-glutamyl cycle. In: Wyngaarden JB, Stanbury JB, Fredrickson DS, Goldstein JL, Brown MS, eds. Metabolic basis of inherited disease. New York: McGraw Hill, 1983;348–359.
72. Smyth MJ. Glutathione modulates activation-dependent proliferation of human peripheral blood lymphocyte populations without regulating their activated function. J Immunol 1991;146:1921–1927.
73. Liang SM, Liang CM, Hargrove ME, Ting CC. Regulation by glutathione of the effect of lymphokines on differentiation of primary activated lymphocytes J Immunol 1991;146:1909–1913.
74. Dröge W, Pottmeyer GC, Schmidt H, Nick S. Glutathione augments the activation of cytotoxic T lymphocytes in vivo. Immunobiology 1986;172:151–156.
75. Gmünder H, Roth S, Eck HP, Gallas H, Mihm S, Dröge W. Interleukin-2 mRNA expression, lymphokine production and DNA synthesis in glutathione-depleted T cells. Cell Immunol 1990;130:520–528.
76. Liang CM, Lee N, Cattell D, Liang SM. Glutathione regulates interleukin-2 activity on cytotoxic T-cells. J Biol Chem 1989;264; 13519–13523.
77. Cantin A, Larivee P, Begin R. Extracellular glutathione suppresses human lung fibroblast proliferation. Am J Respir Cell Mol Biol 1990; 2:79–85.
78. Fetsch J, Maurer HR. Glutathione: An in vitro granulopoiesis inhibitor at nanomolar concentration, isolated from calf spleen. Exp Hematol 1990;18:322–325.
79. Abate C, Patel L, Rauscher FJ III, Curran T. Redox regulation of fos and jun DNA binding activity in vitro. Science 1990;249:1157–1161.
80. Hentze MW, Rouault TA, Harford JB, Klausner RD. Oxidation-reduction and the molecular mechanism of a regulatory RNA-protein interaction. Science 1989;244:357–359.

81. Keyse SM, Applegate LA, Tromvoukis Y, Tyrrell RM. Oxidant stress leads to transcriptional activation of the human heme oxygenase gene in cultured skin fibroblasts. Mol Cell Biol 1990;10:4967–4969.
82. Najita L, Sarnow P. Oxidation-reduction sensitive interaction of a cellular 50-kDa protein with an RNA hairpin in the 5' noncoding region of the poliovirus genome. Proc Natl Acad Sci USA 1990;87: 5846–5850.
83. Roederer M, Staal F, Raju PA, Ela SW, Herzenberg LA, Herzenberg LA. Cytokine-stimulated human immunodeficiency virus replication is inhibited by N-acetyl-L-cysteine. Proc Natl Acad Sci USA 1990;87: 4884–4888.
84. Rokutan K, Thomas JA, Sies H. Specific S-thiolation of a 30-kDa cytosolic protein from rat liver under oxidative stress. Eur J Biochem 1989;179:233–239.
85. Storz G, Tartaglia LA, Ames BN. Transcriptional regulation of oxidative stress-inducible genes: Direct activation by oxidation. Science 1990;248:189–194.
86. Cantin AM, Hubbard RC, Crystal RG. Glutathione deficiency in the epithelial lining fluid of the lower respiratory tract in idiopathic pulmonary fibrosis. Am Rev Respir Dis 1989;139:370–372.
87. Cantin AM, North SL, Hubbard RC, Crystal RG. Normal alveolar epithelial lining fluid contains high levels of glutathione. J Appl Physiol 1987;63:152–157.
88. Buhl R, Jaffe HA, Holroyd KJ, et al. Systemic glutathione deficiency in symptom-free HIV-seropositive individuals. Lancet 1989;2:1294–1298.
89. Buhl R, Jaffe HA, Holroyd KJ, et al. Glutathione deficiency and HIV [Letter]. Lancet 1990;335:546.
90. Eck HP, Gmünder H, Hartmann M, Petzoldt D, Daniel V, Dröge W. Low concentrations of acid-soluble thiol (cysteine) in the blood plasma of HIV-1-infected patients. Biol Chem Hoppe Seyler 1989; 370:101–108.
91. Kalebic T, Kinter A, Poli G, Anderson ME, Meister A, Fauci AS. Suppression of human immunodeficiency virus expression in chronically infected monocytic cells by glutathione, glutathione ester, and N-acetylcysteine. Proc Natl Acad Sci USA 1991;88:986–990.
92. Durand RE, Olive PE. Flow cytometry techniques for studying cellular thiols. Radiat Res 1983;95:456–470.
93. Poot M, Verkerk A, Koster JF, Jongkind JF. De novo synthesis of glutathione in human fibroblasts during in vitro ageing and in some metabolic diseases as measured by a flow cytometric method. Biochim Biophys Acta 1986;883:580–584.
94. Treumer J, Valet G. Flow-cytometric determination of glutathione alterations in vital cells by o-phthaldialdehyde (OPT) staining. Exp Cell Res 1986;163:518–524.
95. Rice GC, Bump EA, Shrieve DC, Lee W, Kovacs M. Quantitative analysis of cellular glutathione in Chinese hamster ovary cells by flow cytometry utilizing monochlorobimane: Some applications to radiation and drug resistance in vitro and in vivo. Cancer Res 1986;46:1-6.
96. Cook JA, Iype SN, Mitchell JB. Differential specificity of monochlorobimane for isozymes of human and rodent glutathione s-transferases. Cancer Res 1991;51:1606–1612.
97. Cook JA, Pass HI, Russo A, Iype S, Mitchell JB. Use of monochlorobimane for glutathione measurements in hamster and human tumor cell lines. Int J Radiat Oncol Biol Phys 1989;16:1321–1324.
98. Hedley DW, Hallahan AR, Tripp EH. Flow cytometric measurement of glutathione content of human cancer biopsies. Br J Cancer 1990;61: 65–68.
99. Kavanagh TJ, Martin GM, Livesey JC, Rabinovitch PS. Direct evidence of intercellular sharing of glutathione via metabolic cooperation. J Cell Physiol 1988;137:353–359.
100. Shrieve DC, Bump EA, Rice GC. Heterogeneity of cellular glutathione among cells derived from a murine fibrosarcoma or a human renal cell carcinoma detected by flow cytometric analysis. J Biol Chem 1988;263:14107–14114.
101. Ublacker GA, Johnson JA, Siegel FL, Mulcahey RT. Influence of glutathione S-transferases on cellular glutathione determination by flow cytometry using monochlorobimane. Cancer Res 1991;51:1783–1788.
102. Woronicz JD, Rice GC. Simple modification of a commercial flow cytometer to triple laser excitation. Simultaneous five-color fluorescence detection. J Immunol Methods 1989;120:291–296.
103. Radkowsky AE, Kosower EM. Bimanes. 17. (Haloalkyl)-1,5-diazabicyclo[33.0] octadienediones (halo-9,10-dioxa-bimanes): Reactivity toward the tripeptide thiol, glutathione. J Am Chem Soc 1986;108: 4527–4531.
104. Poot M, Kavanagh TJ, Kang HC, Haugland RP, Rabinovitch PS. Flow cytometric analysis of cell cycle-dependent changes in cell thiol level by combining a new laser dye with Hoechst 33342. Cytometry 1991;12:184–187.
105. Picket CB, Lu AYH. Glutathione-S-transferases: Gene structure regulation and biological function. Annu Rev Biochem 1989;58:743–764.
106. Jones SM, Brooks BA, Langley SC, Idle JR, Hirom PC. Glutathione transferase activities of cultured human lymphocytes. Carcinogenesis 1988;9:395–398.
107. Jones SM, Idle JR, Hirom PC. Differential expression of glutathione transferases by native and cultured human lymphocytes. Biochem Pharmacol 1988;37:4586–4590.
108. Seidegård J, De Pierre JW, Birberg W, Pilotti A, Pero RW. Characterization of soluble glutathione transferase activity in resting mononuclear leukocytes from human blood. Biochem Pharmacol 1984;33: 3053–3058.
109. Seidegård J, Pero RW, Markowitz MM, Roush G, Miller DG, Beattie EJ. Isoenzyme(s) of glutathione transferase (class Mu) as a marker for the susceptibility to lung cancer: A follow up study. Carcinogenesis 1990;11:33–36.
110. Wiencke JK, Kelsey KT, Lamela RA, Toscano WJ. Genetic polymorphisms in carcinogen metabolism predict substrate-induced cytogenetic damage in humans. Prog Clin Biol Res 1990;340B:137–147.
111. Seidegård J, Pero RW, Stille B. Identification of the trans-stilbene oxide-active glutathione transferase in human mononuclear leukocytes and in liver as GST1. Biochem Genet 1989;27:253–261.
112. Kavanagh TJ, Martin GM, El-Fouly MH, Trosko JE, Chang C-C, Rabinovitch PS. Flow cytometry and scrape-loading/dye transfer as a rapid quantitative measure of intercellular communication in vitro. Cancer Res 1987;47:6046–6051.
113. Tietze F. Enzymatic method for quantitative determination of nanogram amounts of total and oxidized glutathione. Application to mammalian blood and other tissues. Anal Biochem 1969;27:502–522.
114. Baker MA, Cerniglia GJ, Zaman A. Microtiter plate assay for the measurement of glutathione and glutathione disulfide in large numbers of biological sample. Anal Biochem 1990;190:360–365.
115. Watson JV, Dive C, Workman P. Measurement of dynamic cellular events. In: Ormerod MG, ed. Flow cytometry: a practical approach. Oxford: IRL Press, 1990;241–264.
116. Fidelus RK. The generation of oxygen radicals: a positive signal for lymphocyte activation. Cell Immunol 1988;113:175–182.
117. Fidelus RK, Ginouves P, Lawrence D, Tsan MF. Modulation of intracellular glutathione concentrations alters lymphocyte activation and proliferation. Exp Cell Res 1987;170:269–275.
118. Fidelus RK, Tsan MF. Enhancement of intracellular glutathione promotes lymphocyte activation by mitogen. Cell Immunol 1986;97:155–163.
119. Fischman CM, Udey MC, Kurtz M, Wedner HJ. Inhibition of lectin-induced lymphocyte activation by 2-cyclohexene-1-one: Decreased intracellular glutathione inhibits an early event in the activation sequence. J Immunol 1981;127:2257–2262.
120. Hamilos DL, Wedner HJ. The role of glutathione in lymphocyte activation. I. Comparison of inhibitory effects of buthionine sulfoximine and 2-cyclohexene-1-one by nuclear size transformation. J Immunol 1985;135:2740–2747.
121. Hamilos DL, Zelarney P, Mascali JJ. Lymphocyte proliferation in glutathione-depleted lymphocytes: Direct relationship between gluta-

thione availability and the proliferative response. Immunopharmacology 1989;18:223–235.
122. Lacombe P, Kraus L, Fay M, Pocidalo J-J. Glutathione status during the mitogenic response of rat splenocytes. Effects of oxygen concentration: FO2 21% versus FO2 7%. Biochimie 1986;68:555–563.
123. Lacombe P, Kraus L, Fay M, Pocidalo J-J. Glutathione status of rat thymocytes and splenocytes during the early events of their ConA proliferative responses. Biochimie 1987;69:37–44.
124. Shaw JP, Chou I. Elevation of intracellular glutathione content associated with mitogenic stimulation of quiescent fibroblasts. J Cell Physiol 1986;129:193–198.
125. Traganos F, Darzynkiewicz Z, Sharpless T, Melamed MR. Simultaneous staining of ribonucleic and deoxyribonucleic acids in unfixed cells using acridine orange in a flow cytofluorometric system. J Histochem Cytochem 1977;25:46–52.
126. Freed BM, Lempert N, Lawrence DA. The inhibitory effects of N-ethylmaleimide, colchicine and cytochalasins on human T cell functions. J Immunopharmacol 1989;11:459–465.
127. Pettit CM, Hall ND. Surface thiol group involvement in neutrophil and monocyte activation. Biochem Soc Trans 1990;18:305–306.
128. Lee F, Siemann DW. Isolation by flow cytometry of a human ovarian tumor cell subpopulation exhibiting a high glutathione content phenotype and increased resistance to adriamycin. Int J Radiat Oncol Biol Phys 1989;16:1315–1319.
129. Rabinovitch PS, Kubbies M, Chen YC, Schindler D, Hoehn H. BrdU-Hoechst flow cytometry: A unique tool for quantitative cell cycle analysis. Exp Cell Res 1988;174:309–318.
130. Paradiso AM, Tsien RY, Machen TE. Digital image processing of intracellular pH in gastric oxyntic and chief cells. Nature 1987;325:447–450.
131. Musgrove E, Rugg C, Hedley D. Flow cytometric measurement of cytoplasmic pH: A critical evaluation of available fluorochromes. Cytometry 1986;7:347–355.
132. Cook JA, Fox MH. Intracellular pH measurements using flow cytometry with 1,4-diacetoxy-2,3-dicyanobenzene. Cytometry 1988; 9:441–447.